

1 **Overview towards improved understanding of the mechanisms leading to heavy**
2 **precipitation in the Western Mediterranean: lessons learned from HyMeX**

3
4 ¹Samira Khodayar, ²Silvio Davolio, ³Paolo Di Girolamo, ⁴Cindy Lebeau-pin Brossier,
5 ⁵Emmanouil Flaounas, ⁴Nadia Fourrie, ^{6,7} Keun-Ok Lee, ⁴Didier Ricard, ⁴Benoit Vie,
6 ⁴Francois Bouttier, ⁸Alberto Caldas-Alvarez, ⁴Veronique Ducrocq

7
8 ¹Mediterranean Centre for Environmental Studies (CEAM), Valencia, Spain

9 ²National Research Council of Italy, Institute of Atmospheric Sciences and Climate, (CNR-ISAC), Bologna,
10 Italy

11 ³Scuola di Ingegneria, Università degli Studi della Basilicata (SI-UNIBAS), Potenza, Italy

12 ⁴CNRM, Université de Toulouse, Météo-France, CNRS, Toulouse, France

13 ⁵Institute of Oceanography, Hellenic Centre for Marine Research (HCMR), Athens, Greece

14 ⁶Laboratoire d'Aérogologie, Université de Toulouse, CNRS, UPS, Toulouse, France

15 ⁷Laboratoire de L'Atmosphère et des Cyclones, UMR 8105 (CNRS, Université de La Réunion, Météo-
16 France), Saint Denis, France

17 ⁸Institute of Meteorology and Climate Research (IMK-TRO), Karlsruhe Institute of Technology (KIT),
18 Karlsruhe, Germany

19
20
21
22 Submitted to Atmospheric Chemistry and Physics (ACP)

23
24
25 * Corresponding author. E-mail address: khodayar_sam@gva.es (S. Khodayar)

26 Mediterranean Centre for Environmental Studies (CEAM),

27 Technological Park, Charles R. Darwin Street, 14 46980 - Paterna - Valencia - Spain

28 **Abstract**

29 Heavy precipitation (HP) constitutes a major meteorological threat in the western
30 Mediterranean (WMed). Every year, recurrent events affect the area with fatal
31 consequences on infrastructure and personal losses. Despite this being a well-known
32 issue, widely investigated in the past, still, open questions remain. Particularly, the
33 understanding of the underlying mechanisms and the modelling representation of the
34 events must be improved. One of the major goals of the Hydrological cYcle in the
35 Mediterranean eXperiment (HyMeX; 2010-2020) has been to advance knowledge on this
36 topic. In this article, we present an overview of the most recent lessons learned from
37 HyMeX towards an improved understanding of the mechanisms leading to HP in the
38 WMed.

39 The unique network of instruments deployed, the use of finer model resolutions and of
40 coupled models, provided an unprecedented opportunity to validate numerical model
41 simulations, develop improved parameterizations, designing high-resolution ensemble
42 modelling approaches and sophisticated assimilation techniques across scales.

43 All in all, HyMeX and particularly the science team heavy precipitation favoured the
44 evidencing of theoretical results, the enrichment of our knowledge on the genesis and
45 evolution of convection in a complex topography environment, and the improvement of
46 precipitation forecasts. Illustratively, the intervention of cyclones and warm conveyor
47 belts in the occurrence of heavy precipitation has been pointed out, the crucial role of
48 the spatio-temporal distribution of the atmospheric water vapor for the understanding
49 and accurate forecast of the timing and location of deep convection has been evidenced,
50 as well as the complex interaction among processes across scales. The importance of
51 soil and ocean conditions and the interactions among systems were highlighted and such
52 systems were specifically developed in the framework of HyMeX to improve the realism
53 of weather forecasts. Furthermore, the benefits of cross-disciplinary efforts within HyMeX
54 have been a key asset in bringing a step forward our knowledge about heavy
55 precipitation in the Mediterranean region.

56

57

58

59

60

61 **1. Introduction and Motivation**

62 A 10-Year Multidisciplinary Program on the Mediterranean Water Cycle, HyMeX,
63 Hydrological Cycle in the Mediterranean Experiment (Drobinski et al., 2014), has come
64 to an end (2010-2020). With the main goal to advance the scientific knowledge of the
65 Mediterranean water cycle variability and to improve the process-based and regional
66 climate models, different temporal scales are considered, from weather-scale to the
67 seasonal and interannual scales. Special focus is put on the hydrometeorological
68 extremes and consequent social and economic impacts, as well as the vulnerability and
69 the adaptation capacity of the Mediterranean population under Climate Change.

70

71 The unique character of the Mediterranean basin and surrounding countries resulting
72 from the geographical location, climatic conditions, and topography, makes the region
73 prone to extreme phenomena; heavy precipitation and flash floods, as well as heat
74 waves and drought (e.g., Mariotti, 2010). The region, defined as one of the two main “hot
75 spots” of climate change (Giorgi, 2006; IPCC, 2013), is in a transition area, therefore,
76 very sensitive to global climate change at short and long-time scales. An increase in
77 interannual rainfall variability, strong warming and drying in addition to a significant
78 population growth are projected for the coming future. Despite the overall Mediterranean
79 climate drying, under climate change, intensity of heavy precipitation events (HPEs) is
80 expected to increase (Planton et al., 2016; Jacob et al., 2013; Drobinski et al., 2016;
81 Colmet-Daage et al., 2017; Tramblay and Somot, 2018; Giorgi et al., 2019). In this
82 context, threats posed from the expected increase in frequency and intensity of events
83 conducive to floods and droughts (Gao et al., 2006; Orłowsky and Seneviratne, 2011)
84 are seen with great concern. Countries surrounding the Mediterranean basin already
85 suffer water problems in relation to water shortages and floods. Food security could also
86 become an issue (Nelson et al., 2010).

87

88 HPEs and the associated flash floods are the most dangerous meteorological hazards
89 affecting the Mediterranean countries in terms of mortality, and hundreds of millions of
90 euros in damages are registered every year (Llasat et al., 2010, 2013; Doocy et al.,
91 2013). The Mediterranean basin and particularly the surrounding mountainous coastal
92 regions are often affected by these phenomena, regularly in the autumn period. The
93 Mediterranean Sea, acting as a heat and moisture source, and the steep orography,
94 triggering convection, are key aspects determining the occurrence of heavy precipitation
95 in the region which is mainly of convective nature (Funatsu et al., 2008; Dayan et al.,

96 2015). Rainfall accumulations greater than 100-150 mm may be expected in less than a
97 day or even just a few hours resulting mostly from quasi-stationary mesoscale convective
98 systems (MCSs; Lee et al., 2018, 2017, 2016; Duffourg et al 2018; Buzzi et al., 2014).
99 Such rainfall accumulations are favoured by a slowly evolving synoptic situation,
100 characterized by an upper-level trough and consequent cyclogenesis that induces
101 advection of warm and moist air from the Mediterranean Sea (Duffourg and Ducrocq,
102 2011) to the coasts through marine low-level jets (Homar et al., 1999; Jansa et al., 2001;
103 Nuissier et al., 2011; Ricard et al., 2012; Khodayar et al., 2016b). Strong wind with high
104 sea surface temperature (SST) governs evaporation, which moistens and warms the
105 lowest levels of the atmosphere, thus increasing instability and finally often enhancing
106 the convection intensity (Xie et al., 2005, Lebeaupin et al., 2006; Stocchi and Davolio,
107 2017, Rainaud et al., 2017; Senatore et al., 2020a). Low-level convergence over the sea,
108 cold pools beneath the convective systems, or topographic lifting when encountering the
109 coastal mountains trigger deep convection, forcing the lift of the conditionally unstable
110 low-level flow. The synoptic-scale situations associated with these episodes are
111 generally well-known and well represented in numerical weather prediction (NWP) model
112 simulations. Nevertheless, in the last few years, additional knowledge has been gained
113 in the field. Vries (2020) presented for the first time a global and systematic
114 climatological analysis of the Rossby Wave Breaking (RWB) and intense moisture
115 transport, and their linkage to extreme precipitation events (EPEs), with the findings of
116 this study contributing to an improved understanding of the atmospheric processes that
117 lead to EPEs. Mastrantonas et al (2021) demonstrated that a clustering combination of
118 sea level pressure (SLP) and geopotential height at 500 hPa (Z500), increases by more
119 than three the conditional probability of EPEs, which could result critical for extended-
120 range forecasts. Grazzini et al. (2021) further investigated the relation between EPEs
121 and Rossby Wave Packets (RWPs), showing the evolution and properties of precursor
122 RWPs to be key for the categorization of EPEs. Despite the improved understanding,
123 the accuracy of forecasts is still insufficient to adequately assess timing, location and
124 intensity of rainfall and flash flooding in certain situations, which is a key step towards
125 prevention and mitigation. This is mostly in relation to (a) model limitations in terms of
126 predictability of small-scale processes (e.g., convection, turbulence) and feedbacks
127 (e.g., soil, atmosphere, ocean) and their non-linear interaction across scales, (b) lack of
128 knowledge regarding underlying mechanisms, and (c) absence of adequate
129 observations to help us advance our understanding and improving model capabilities.
130 This issue is one of the main objectives of the HyMeX international programme, and of
131 its associated first special observation period (SOP1; Ducrocq et al., 2014; Jansa et al.,
132 2014; Ferreti et al., 2014), from 5 September to 6 November 2012, dedicated to heavy

133 precipitation and flash flooding. Because of the large number of instruments deployed,
134 the unprecedented high spatial-temporal coverage achieved and the quality of the
135 derived observations, the SOP1 has offered a unique opportunity to improve
136 understanding and advance documenting high-impact weather events. This is in addition
137 to the significant progress achieved in the last decade through the development of
138 convection-permitting models, whose benefit has been sufficiently demonstrated
139 (Richard et al., 2007; Fosser et al., 2014, Prein et al., 2015; Clark et al, 2016, among
140 others) and it is widely used nowadays from the scientific community.

141 The major goal of this article is to expose an overview on some of the recent years' main
142 achievements towards better understanding of the mechanisms leading to heavy
143 precipitation in the WMed in the framework of the HyMeX international programme.
144 Advances regarding improved understanding of the mechanisms governing the initiation
145 and intensification of precipitating systems producing large amounts of rainfall are
146 thoroughly discussed in terms of in situ observations and high-resolution modelling
147 systems, as well as the synergetic use of both to help us bridge knowledge gaps. An
148 intensive observation period IOP16, which took place during the SOP1, is taken as a
149 paradigm to illustrate some of the main HyMeX results in the field of heavy precipitation.
150 This paper is structured as follows: in section 2 we describe the general conditions
151 leading to HP during the SOP1 period, the state-of-the-art of the observational networks
152 deployed in this time, as well as the modelling strategy developed. Additionally, the
153 IOP16, which has been used throughout the paper for illustrating some of the results is
154 presented. In section 3, the main advances regarding HP understanding and modelling
155 are presented, including the large-scale dynamics, advances in moist process
156 understanding, low-level dynamics, the impacts of the land and the sea surfaces and
157 microphysics. Section 4 is devoted to the examination of the improvements in the multi-
158 scale modelling of HP and in section 5 some conclusions and recommendations are
159 summarized.

160

161 **2. Heavy precipitation during the HyMeX SOP1 period**

162 The SOP1 campaign took place in 2012, from 5 September to 6 November, when the
163 probability of HPE occurrence in the north-western Mediterranean is the highest. About
164 30% of the days in this period experienced, indeed, rainfall accumulations over 100 mm
165 somewhere in the investigation domain. Twenty Intensive Observation Periods (IOPs)
166 were launched during the campaign, most of them occurring in the period after mid-
167 October to the end of the SOP1 (Ducrocq et al., 2014). This agrees with the monthly
168 precipitation totals being close to the climatological values in September, but well above

169 in October (Khodayar et al., 2016b). Most IOPs did not affect a single site but
170 encompassed several regions of the north-western Mediterranean. The most affected
171 sites were the Cévennes-Vivarais (CV), including the Massif Central and the French
172 Southern Alps, as well as the Liguria-Tuscany (LT) region in Italy.

173 **2.1. State-of-the-art observational capabilities and modelling activities**

174 More than 200 research instruments were deployed over the WMed Sea and surrounding
175 countries, namely Spain, France, and Italy to ensure a close observation of the
176 precipitating systems and a fine-scale survey of the upstream meteorological conditions
177 over the Mediterranean. Ducrocq et al. (2014) provides a comprehensive description of
178 the observing systems deployed during the SOP1. Furthermore, this unique network of
179 instruments provided an unprecedented opportunity to validate more accurately NWP
180 model simulations, to develop novel data assimilation techniques and to improve model
181 parameterizations with the purpose of better predicting the evolution of the environment
182 across scales.

183 **2.1.1 Ground-based, airborne, and seaborne observations**

184 One unique aspect of HyMeX-SOP1 was represented by the availability of a large
185 ensemble of ground-based and airborne instruments, covering a major portion of the
186 WMed and its surrounding coastal regions in France, Italy, and Spain. The observational
187 domain of HyMeX-SOP1 was defined to include the area with the highest occurrence of
188 HPEs and being within the ranges of aircraft flight endurance. Within this large domain,
189 five measurement sites including advanced research instruments were established, i.e.
190 the Cévennes-Vivarais (CV) and the Corsica (CO) sites, the Central Italy (CI) and
191 Northeastern Italy (NEI) sites, and the Spanish Balearic Islands (BA) site including
192 Menorca and Mallorca (Ducrocq et al., 2014). Most sites were equipped with soil
193 moisture sensors, turbulence or energy balance stations, microwave radiometers, lidars,
194 radars (cloud, precipitation and/or wind) and radiosonde launching facilities, in addition
195 to the operational meteorological and hydrological ground networks covering the entire
196 SOP1 domain. Thus, an unprecedented dense network of rain gauges was available
197 over France, Italy, and Spain, with a density of about one hourly rain gauge per 180 km².
198 This network operated in combination with a radar network including a variety of S-band,
199 C-band Doppler (two of them being polarimetric) and X-band radars (one of them being
200 polarimetric). A similarly dense network of Global Positioning System (GPS) stations was
201 also established, with stations covering the north-western Mediterranean basin and
202 including measurements from 25 European, national, and regional GPS networks (Bock
203 et al., 2016).

204 Three aircrafts participated in the field campaign: the French ATR42, the French Falcon
205 20 (operated by SAFIRE (Service des Avions Français Instrumentés pour la Recherche
206 en Environnement)) and the German Do128 (Corsmeier et al., 2001). The ATR42
207 involvement was primarily aimed to characterize the origin and transport pattern of water
208 vapor and aerosol in pre-convective conditions and their link with heavy precipitating
209 systems. Its main payload was the airborne dial LEANDRE 2, capable of profiling water
210 vapor mixing ratio above or beneath the aircraft. The F20 aircraft primary mission was
211 the characterization of the microphysical and kinematic processes taking place within
212 convective precipitating systems, this objective being pursued based on the use of
213 advanced microphysical in situ probes and the 95-GHz Doppler cloud radar RASTA
214 (Radar Aéroporté et Sol de Télédétection des propriétés nuAgeuses, Protat et al., 2009).
215 Furthermore, the German Do 128 research aircraft was equipped with fast sensors to
216 measure turbulent fluxes, water vapor inlet, and stable water isotope measurements
217 (Sodemann et al., 2017) with the primary goal of monitoring upstream low-level
218 conditions before and during HPEs and investigating the orographic and thermal impact
219 of the island on the initiation and evolution of diurnal convective activity.

220 During HyMeX-SOP1 Boundary Layer Pressurized Balloons (BLPBs) were also
221 launched from Menorca, flying at a nearly constant height (Doerenbecher et al., 2016)
222 and providing Lagrangian trajectories of specific humidity, temperature, pressure, and
223 horizontal wind.

224

225 Two ground-based Raman lidars were involved, namely the system BASIL (Di Girolamo
226 et al., 2009), deployed in Candillargues (Southern France) and the system WALI (Water-
227 vapour Raman Lidar; Chazette et al., 2016), deployed in Ciutadella (Menorca, Balearic
228 Islands). Both systems provided long-term records of high-resolution and accurate
229 humidity measurements, both in daytime and night-time, throughout the duration of
230 HyMeX-SOP1.

231

232 At sea, several platforms were deployed to monitor the ocean upper-layer and the
233 exchanges with the atmosphere (Ducrocq et al., 2014, Lebeaupin Brossier et al., 2014,
234 Rainaud et al., 2015). Two Météo-France moored buoys, LION (4.7°E–42.1°N) and
235 AZUR (7.8°E–43.4°N), routinely provide the 2 m-temperature, humidity, 10 m-wind
236 speed, direction, and gust intensity, mean sea level pressure and sea surface
237 parameters (SST, wave height and period). They were equipped with additional sensors
238 for HyMeX with radiative flux measurements, raingauges, a thermosalinograph
239 measuring the near-surface temperature and salinity, and a thermobathymetric chain

240 giving the ocean temperature between 5 and 250 m-depth. During SOP1, up to five
241 gliders monitored the area simultaneously, providing 0–1000 m profiles along repeated
242 transects. Observations from ships include CTD profiles (up to 200 m-depth) and
243 radiosoundings from the port-tender Le Provence sent in the Gulf of Lion for 3 IOPs
244 (IOP7, IOP12 and IOP16). Finally, the freighter Marfret-Niolon that regularly linked
245 Marseille (France) with Algiers (Algeria), was equipped for HyMeX with the SEOS (Sea
246 Embedded Observation System; <http://dx.doi.org/10.6096/MISTRALS-HYMEX.748>)
247 station, measuring air temperature, relative humidity, pressure, wind, and SST. Another
248 sensor provided measurements of sea temperature at almost 3 m-depth, using a high-
249 quality temperature probe (TRANSMED data: [http://dx.doi.org/10.6096/MISTRALS-](http://dx.doi.org/10.6096/MISTRALS-HYMEX.973)
250 [HYMEX.973](http://dx.doi.org/10.6096/MISTRALS-HYMEX.973)), backed by a thermosalinograph that also provided in-situ salinity.

251 **2.1.2 HyMeX modelling strategy**

252 Despite significant efforts to improve the skill of forecasts, the forecasting accuracy has
253 been proved still insufficient in terms of amount, timing, and location of heavy
254 precipitation. The design of the HyMeX modelling strategy considered three key issues
255 proved to be relevant to reduce modelling uncertainty: (a) to be consistent with the
256 observation strategy, (b) to integrate numerical models of the atmosphere, ocean, and
257 land and (c) to include models of the climate system to cover all scales of time and space.
258 Moreover, through the refinement of model grids and the development of convection-
259 permitting NWP systems and Regional Climate Models (RCM), significant progress has
260 been made to improve the simulations of HPEs, the knowledge of the relevant processes
261 and their interactions across scales, as well as to reduce the large uncertainties on the
262 future evolution under climate change. The use of finer-scale and coupled models
263 representing more accurately the atmosphere-ocean-land systems and their
264 interactions, and/or the detailed validation using the SOP1 measurements allowed the
265 development of improved parameterizations of physical processes, the design of high-
266 resolution ensemble modelling approaches with greater number of ensemble members,
267 and a more sophisticated and efficient use of observations for assimilation purposes.

268 Profiting from these efforts, the HyMeX community has made relevant advances in
269 process knowledge and prediction of heavy precipitation. Some of these advances are
270 discussed and illustrated in the coming sections using the IOP16, which is introduced in
271 the following.

272 **2.2. Illustrative case: IOP 16**

273 The IOP 16 is a well-documented and widely investigated event observed in the period
274 25-29 October 2012 over the WMed region. IOP 16 was one of the best equipped
275 observational periods in terms of instrumental coverage during HyMeX-SOP1 (Figure 1).

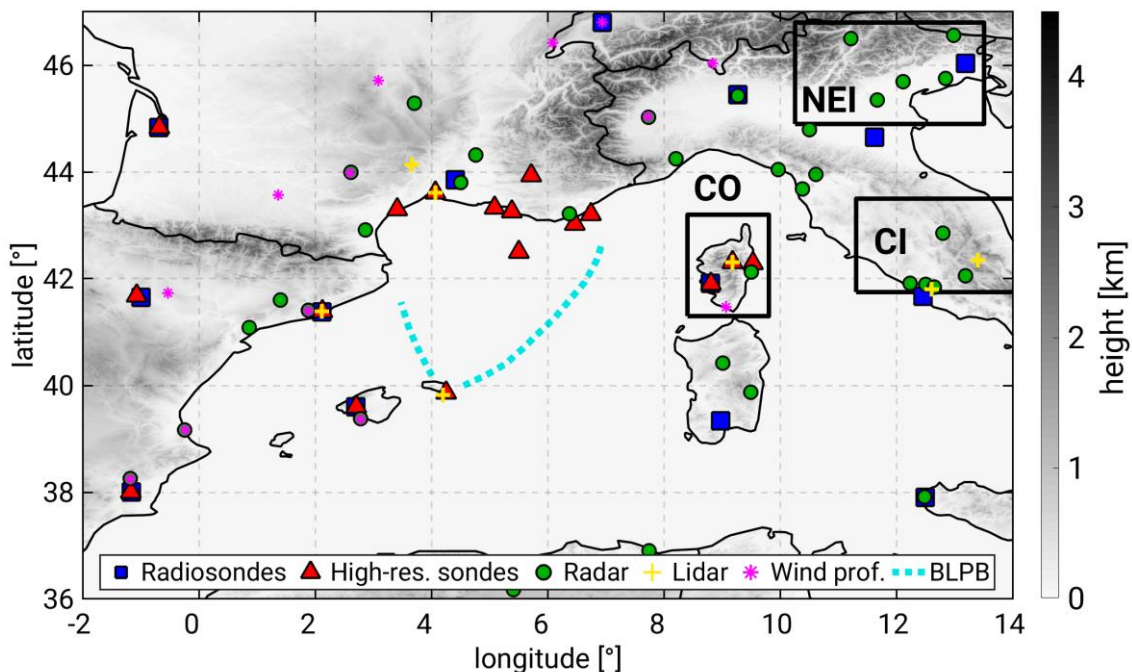
276 Most ground-based and air-borne instrumentation were successfully operational,
277 providing high quality data, with almost all the on-demand SOP1 instruments involved.
278 Benefiting from this large observational dataset, an extensive number of modelling
279 activities focused on the IOP 16, with the purpose of investigating different issues related
280 with the occurrence of heavy precipitation, such as the impact of the turbulence
281 representation on the sensitivity of the simulated convective systems (Martinet et al.,
282 2017), the underlying mechanisms of offshore deep convection initiation and
283 maintenance (Duffourg et al., 2016), some assimilation or pre-assimilation experiments
284 (Borderies et al., 2019a), the impact of fine-scale air-sea interactions and coupled
285 processes on heavy precipitation (Rainaud et al., 2017), or novel Large Eddy Simulation
286 (LES) of a HPE (Nuissier et al., 2020).

287 This event was associated with a propagating cyclone and was observed in two
288 dedicated periods: (a) the IOP16a (25–26 October), characterized by heavy
289 precipitation over CV and LT, when several quasi-stationary MCSs developed, two of
290 them over the sea, with subsequent heavy precipitation over the French and Italian
291 coasts on 26 October 2012, and (b) the IOP16b (27–29 October) characterized by heavy
292 precipitation over CI, NEI, and CO regions.

293 The IOP16a was driven by the presence of a cyclone moving from the easternmost
294 Atlantic to the Pyrenees, followed in phase by a cut-off low, associated with upper-level
295 high potential vorticity values. In the lower troposphere, the cyclone provoked
296 southwesterly advection of moist and warm air above 20 °C. On the morning of the 26
297 October the cyclone was centered over the Pyrenees, forming a convergence line
298 between the southerly flow and the southwesterly colder winds, while over the Tyrrhenian
299 Sea a southerly moist and warm flow from Tunisia to the Gulf of Genoa established
300 (Fourrié et al., 2015).). During the night from the 25th to the 26th of October,
301 and in the following day, several MCSs formed under the influence of the cyclone and
302 within its “comma-shaped” cloud coverage. Such cloud coverage is typically found in
303 mid-latitude storms and owes its shape to warm conveyor belts (WCB; Eckhardt et al.
304 2004; Madonna et al. 2014), i.e. the airstreams that ascend slantwise over the cyclone
305 warm front. All MCSs showed a quasi-stationary behavior, forming first over the sea,
306 between the eastern Spanish coast and the Balearic Islands (Duffourg et al., 2016), and
307 afterwards over the Gulf of Lion where they induced large amounts of precipitation over
308 sea during morning hours.

309 The first MCS split in two. One system (MCS1a) moved towards the southeast of the
310 Massif Central, but progressively decayed producing just orographic rainfall; the second

311 (MCS1b) strengthened and caused a large precipitation accumulation over the Var
 312 region during the afternoon, nearly 150 mm in 24 h, causing two fatalities in the city of
 313 Toulon. A third MCS initiated at about 06:00 UTC on 26 October on the Italian coast of
 314 Liguria. The MCS development occurred also offshore Sardinia and Corsica and reached
 315 central Italy during the evening on 26 October, leading to 250 mm daily precipitation on
 316 this day over Liguria-Tuscany, with local flash flooding. On the same day, over the
 317 Cévennes-Vivarais region, daily precipitation reached 170 mm.
 318 During the second period, 27–28 October 2012, the cyclone centre reached the lowest
 319 pressure of 985 hPa over the Alps (Fig. 2), associated with a clear trough in the upper
 320 troposphere and provoking severe northwesterly/northerly winds advecting cold and dry
 321 air over the WMed Sea and inducing large evaporation and ocean cooling and mixing
 322 (Lebeaupin Brossier et al., 2014; Rainaud et al., 2015, 2017; Seyfried et al., 2018). The
 323 relationship between cyclone dynamics and heavy rainfall during IOP16 is discussed in
 324 detail by Flaounas et al. (2016).
 325



326
 327 **Figure 1:** Location of selected experimental setup during the IOP16, 25-28 Oct. 2012,
 328 including radiosondes and high-resolution sondes, radar, lidar, wind profilers, and
 329 Boundary Layer Pressurized Balloons (BLPB). The position of the GPS receivers can be
 330 found in Figure 3d. The location of the CO, NEI and CI subdomains are indicated with
 331 black boxes.

332

333 **3. Towards improved understanding of the mechanisms leading to heavy**
334 **precipitation in the Western Mediterranean**

335 **3.1 Large-scale dynamics and HPE occurrence**

336 Mediterranean cyclogenesis is typically preceded by the intrusion of upper tropospheric
337 systems such as troughs and cut-off lows. Such systems are typically shown to be direct
338 results of Rossby wave breaking over the Atlantic ocean and be related with high
339 potential vorticity values that trigger cyclogenesis in the Mediterranean due to baroclinic
340 instability (Grams et al., 2011; Raveh-Rubin and Flaounas, 2017). Therefore, most
341 intense Mediterranean cyclones are baroclinic systems with frontal structures and
342 associated airstreams such as dry air intrusions and WCB (Ziv et al. 2009; Flaounas et
343 al. 2015a). In particular, WCBs are associated with stratiform, but also with
344 convective rainfall due to embedded convection within their large-scale ascent branch
345 (Flaounas et al., 2018; Oertel et al., 2019). Such is the case of IOP16, where WCBs and
346 deep convection coexisted to attribute large amounts of rainfall over the western
347 Mediterranean (Figure 2).

348

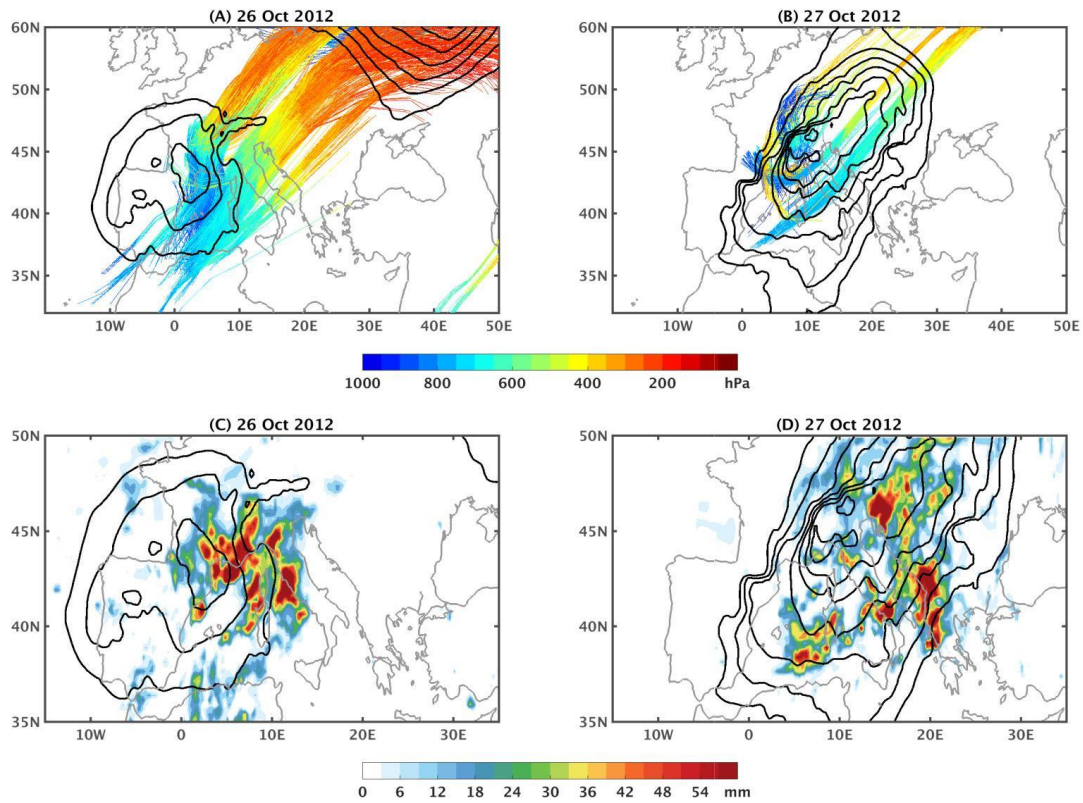
349 Therefore, most intense Mediterranean cyclones are baroclinic systems with frontal
350 structures and associated airstreams such as dry air intrusions and WCB (Ziv et al. 2009;
351 Flaounas et al. 2015a). In particular, WCBs are associated with stratiform, but also
352 with convective rainfall due to embedded convection

353 Several past studies showed that HP in the Mediterranean basin is intertwined with the
354 occurrence of cyclones. Scheffknecht et al. (2017) showed that cyclones are present for
355 all HPEs over the Corsica Island when examining the climatology in the period 1985-
356 2015. Embedded deep convection and WCBs are responsible for the grand majority of
357 total regional precipitation and its extremes (Jansa et al., 2001; Hawcroft et al., 2012;
358 Pfahl et al., 2014; Galanaki et al., 2016; Raveh-Rubin and Wernli, 2015). As a token of
359 cyclones contribution to regional rainfall, Flaounas et al. (2018) showed that the 250
360 most intense systems of the period 2005-2015 were alone responsible for up to a third
361 of the total 11-year precipitation, while climate modelling showed that cyclones
362 contributed from 70% to almost the total of rainfall extremes, depending on the area
363 (Flaounas et al., 2015). Such heavy rainfall events are related to water sources from the
364 Mediterranean Sea, but also from the tropical and extratropical Atlantic Ocean. This is
365 due to cyclogenesis being preceded by Rossby wave breaking over the Atlantic that

366 favours the eastward zonal transport of water vapour from oceanic remote areas,
367 rendering water vapour imports imperative for the formation of heavy rainfall in the
368 Mediterranean (Duffourg and Ducrocq, 2013; Flaounas et al., 2019).

369

370



371

372

373 Figure 2: (a) Sea level pressure (black contours every 3 hPa, outer contour is set at 1005
374 hPa). Coloured lines show the pressure level of the WCB air masses, related to the
375 cyclone. WCBs are calculated using the ECMWF analyses and correspond to air mass
376 trajectories that present an ascent of more than 500 hPa within 48 hours. In panel (a),
377 we show the 48-hour trajectories that correspond to WCBs and where air masses are
378 located close to the cyclones centre at 12:00 UTC, 26 October 2012, between 680 and
379 720 hPa. i.e. within the ascending part of the WCBs (line segments of cyan colours). (b)
380 as in (a), but for 12:00 UTC, 27 October 2012. (c) Colours show daily accumulation of
381 precipitation on 26 October 2012 taken from 3B42 of TRMM. (d) as in (c) for 27 October.
382 Datasets and methods for all panels are detailed in Flaounas et al. (2016).

383

384 **3.2 Advances in moist processes understanding**

385 **3.2.1 Distribution, origin, and transport of the water vapour supply**
386 **to HPEs**

387 The relevance of atmospheric water vapour distribution and stratification in the initiation,
388 intensification, and maintenance of HPEs has been extensively demonstrated (e.g.,
389 Duffourg et al., 2018; Lee et al., 2018), as well as the role of the Mediterranean Sea as
390 a significant heat and moisture source for HPEs in the WMed area (Duffourg and
391 Ducrocq, 2011; Flaounas et al., 2019). The scarcity of water vapour observations at the
392 mesoscale and smaller scales, as well as the model limitations, for example in relation
393 to the adequate spatial and temporal resolution and/or an accurate representation of the
394 vertical stratification, hampered progress in the past. Indeed, our understanding of the
395 variability of water vapour in relation to convection is still far from being complete. Large
396 uncertainties remain regarding the origin, pathways, and timescales of transport of the
397 large amounts of moisture necessary for HPEs in the WMed. The characterization and
398 better understanding of the water vapour supply to HPEs has been a key aspect of the
399 HyMex field campaign and subsequent studies. The unprecedented deployment of
400 instruments during the SOP1 for the monitoring of water vapour dynamics and the
401 posterior cross-validation studies and synergetic use together with models allowed the
402 many advances achieved in this period as described in the following.

403 One of the HyMeX observational highlights has been the dense network of GPS stations,
404 over one thousand ground-based receivers, providing a reprocessed dataset specially
405 produced for the HyMeX SOP (Bock et al., 2016). The large extent and high-density
406 coverage of the reprocessed GPS network allowed a consistent representation of large-
407 scale features, as well as smaller spatial and temporal scales in agreement with high-
408 resolution simulations (Bock et al., 2016). Using the reprocessed integrated water vapour
409 (IWV) GPS data Khodayar et al. (2018) showed that all HPEs within the north-western
410 Mediterranean form in periods/areas characterized by IWV values in the order of 35-45
411 mm after an increase of 10-20 mm, being the most intense events those experiencing a
412 more sudden increase (between 6 to 12 h prior to the event). Bock et al. (2016)
413 demonstrated that regions prone to HPEs in autumn are characterized by high IWV
414 variability up to 8 kg/m².

415 In addition to the unprecedented (in terms of spatial and temporal coverage) amount of
416 information provided by the postprocessed GPS network, modelling studies are helpful
417 for the assessment of potential sources of moisture. Recent advances in this topic
418 showed that the evaporation in the western Mediterranean, in the central Mediterranean,

419 in the North Atlantic, and the advection from the tropical and subtropical Atlantic and
420 Africa constitute the four moisture sources which could explain most of the accumulated
421 precipitation in the WMed (Insua-Costa et al. 2019). The evaporation from the
422 Mediterranean accounts for only about 40% (60%) of the water vapour feeding the deep
423 convection developed over southeastern France when cyclonic (anticyclonic) conditions
424 prevails in the days preceding the event (Duffourg and Ducrocq, 2013). The Atlantic
425 Ocean (Turato et al., 2004; Winschall et al., 2011; Duffourg et al., 2018; Flaounas et al.,
426 2019) and tropical Africa (Krichak et al., 2015; Chazette et al., 2015b; Lee et al., 2016,
427 2017) have been also suggested as potential sources of moisture for HPE occurring in
428 the western Mediterranean. The large-scale uplift of enriched African moisture plume
429 and their role in gradual rain out of the air parcel over southern Italy during IOP13 were
430 highlighted in a modelling study taking advantage of stable water isotopes by Lee et al.
431 (2019). Backward trajectory analysis showed that the large-scale moisture transport
432 takes place during about 3 to 4 days in the warm sector of front, whereas the surface
433 evaporation over the Mediterranean occurs shortly in a few hours to 1 day. Associated
434 with extreme precipitation events over Italy, whether convective or orographic, a recent
435 study by Grazzini et al. (2019) confirmed the systematic occurrence of anomalously high
436 values of meridional Integrated Vapour Transport that sometimes occurs in narrow
437 filament shape regions of high integrated moisture, called atmospheric rivers (Davolio et
438 al., 2020), as during the 2011 Liguria floods (Rebora et al., 2013) or the last extreme
439 storm in October 2018 (Giovannini et al., 2021) and October 2020 (Magnusson et al.,
440 2021).

441 **3.2.2 Assessment of the variability and vertical distribution of the** 442 **atmospheric water vapour**

443 The variability and vertical distribution of the atmospheric water vapour and their
444 accurate representation in models have been demonstrated to play a key role for the
445 timing, location, and intensification of deep convection (e.g., Khodayar et al., 2018), thus
446 for the simulation of HPEs. They have been further identified as responsible for
447 inaccuracies in RCMs when compared against convection-permitting NWP models
448 (Khodayar et al., 2016a). To contribute to the characterization of the water vapour
449 variability, the ground-based WALI in the Balearic Islands, the airborne water-vapour
450 differential absorption lidar LEANDRE 2 on board the ATR42 aircraft, and boundary layer
451 pressurized balloons (BLPB; Doerenbecher et al., 2016) were deployed during the
452 SOP1. Water Vapour Mixing Ratio (WVMR) profiles were measured with a horizontal
453 resolution of 1 km (e.g., Flamant et al., 2015; Flaounas et al., 2016; Chazette et al.,
454 2015a, 2015b; Di Girolamo et al., 2017; Duffourg et al., 2016; Lee et al., 2016, 2017). In

455 a multi-instrument and multi-model assessment of atmospheric moisture variability in the
456 north-western Mediterranean, Chazette et al. (2015b) demonstrated the consistency and
457 self-coherence of these water vapour data sets during the SOP1 pointing out the strong
458 need in assimilating high-resolution water-vapour profiles in the lowest layers as those
459 from lidar instruments. In a multi-scale observational investigation of atmospheric
460 moisture variability in relation to HPEs formation in the same region, Khodayar et al.
461 (2018), profited from the synergetic use of the observational datasets demonstrating that
462 the sampling of spatial inhomogeneities on different scales is crucial for the
463 understanding of the timing and location of deep convection. Furthermore, focusing on
464 the complex island of Corsica during SOP1, multiple observations from the mobile
465 observations platform KITcube (Kalthoff et al., 2013) further demonstrated the benefit of
466 integrated measurement systems (Adler et al., 2015).

467 The ground-based lidar WALI was useful in capturing the moist and deep boundary
468 layers with updrafts reaching up to 2 km in pre-convective environments leading to HPEs,
469 contrary to the dry, shallow boundary layers everywhere else (Khodayar et al., 2018). In
470 Chazette et al. (2015a), the ground-based lidar WALI, additionally captured the
471 increasing moistening of the free troposphere, up to 5 km, prior and in relation to the
472 MCS formation. Furthermore, the specific humidity observations from BLPB and aircraft
473 flights captured spatial inhomogeneities in the lower boundary layer up to 4 g/kg in less
474 than 100 km, which were shown to determine the location of convection initiation
475 (Khodayar et al. 2018).

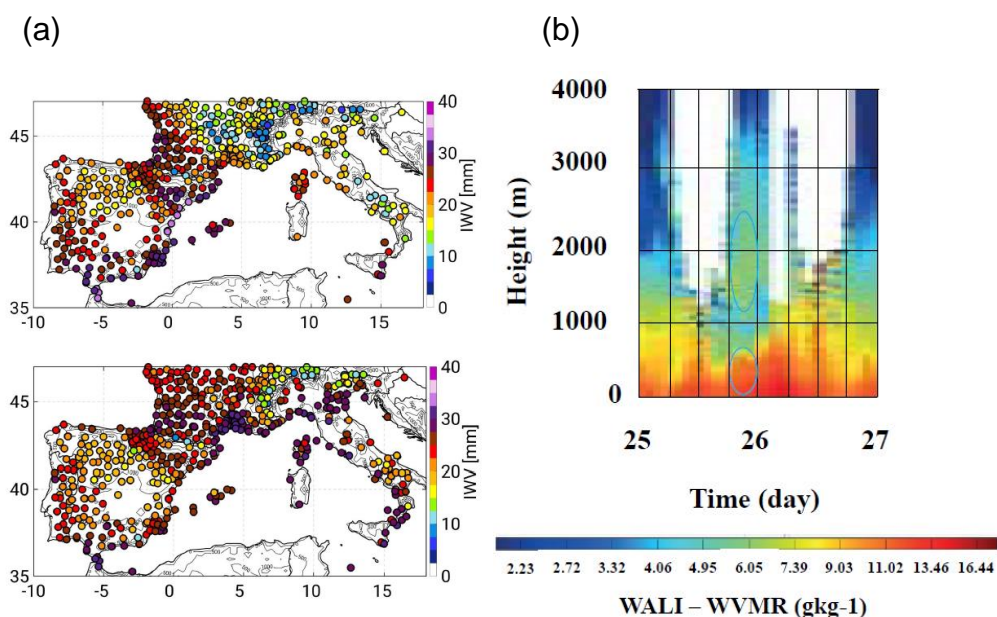
476 Figure 3 illustrates for the IOP16 the complex moisture flow that fed the convective
477 systems, which was effectively monitored by the variety of water vapour profiling sensors
478 involved in combination with backward and forward trajectory analyses from a
479 Lagrangian model (NOAA HYSPLIT Lagrangian trajectory model; Draxler and Hess,
480 1998; Rolph et al., 2017; Stein et al., 2015) and the information derived from the GPS
481 network.

482 In Figure 3a, the spatial distribution of the 24 h-averaged GPS-derived IWV on 25 and
483 26 October 2012 shows initially higher atmospheric moisture content in the western area,
484 where convection initiation takes place, whereas on the next period the humid air mass
485 has advanced eastwards. The water vapor mixing ratio as measured by WALI in
486 Ciutadella (Menorca) (Figure3b) reveals the presence of two distinct humid layers in the
487 time interval 18:00–00:00 UTC on 25 October 2012: a surface layer extending up to
488 about 0.6 km, with mixing ratio values up to $\sim 12 \text{ g kg}^{-1}$, and an elevated layer extending
489 from 1.1 to 2.5 km, with mixing ratio values up to $6\text{--}7 \text{ g kg}^{-1}$. The 24 h forward trajectory

490 analysis starting in Ciutadella at 21:00 UTC on 25 October 2012 at the altitudes of the
 491 observed humidity layers (Figure 3c) shows the northward movement of the surface
 492 humid layer, while air masses within the elevated humidity layer moved north-eastward.
 493 The latter are plausibly related to the inflow branch of WCBs, i.e., the blue part of the air
 494 mass trajectories in Figure 2. The surface humid layer overpassed Candillargues about
 495 15–21 hours later, as proved by the mixing ratio profile measurements carried out by
 496 BASIL and illustrated in Figure 3e, possibly feeding the MCS forming close to the cyclone
 497 centre over the Cévennes-Vivarais region in the morning of 25 October. Indeed, the
 498 water vapour profile shown in Figure 3e is consistent with the one provided by LEANDRE
 499 2, on board the ATR42 aircraft that flew over the WMed (Figure 12 in Flaounas et al.,
 500 2016). The 24 h forward trajectory analysis also reveals that air masses within the
 501 elevated humid layer overpassed the Gulf of Lion, possibly ending up with feeding the
 502 offshore MCS system. Figure 3d additionally illustrates the 200-h back-trajectory
 503 analysis ending in Minorca at 21:00 UTC on 25 September 2012 at the altitudes (500 m
 504 and 2000 m) where the two humid layers were observed, revealing that air masses within
 505 the surface humidity layer originated over the tropical Atlantic Ocean approximately 8
 506 days earlier and overpassed Morocco and Southern Spain, slowly subsiding (in the last
 507 72-96 hours before the formation of them MCS) upon reaching the Mediterranean basin
 508 from an altitude of 1000 m down to 500 m, whereas the air masses within the elevated
 509 humid layer originated over Central Africa (Northern Mali) approximately 3 days earlier
 510 and transited over Mauritania and Morocco before reaching the Balearic Islands.

511

512



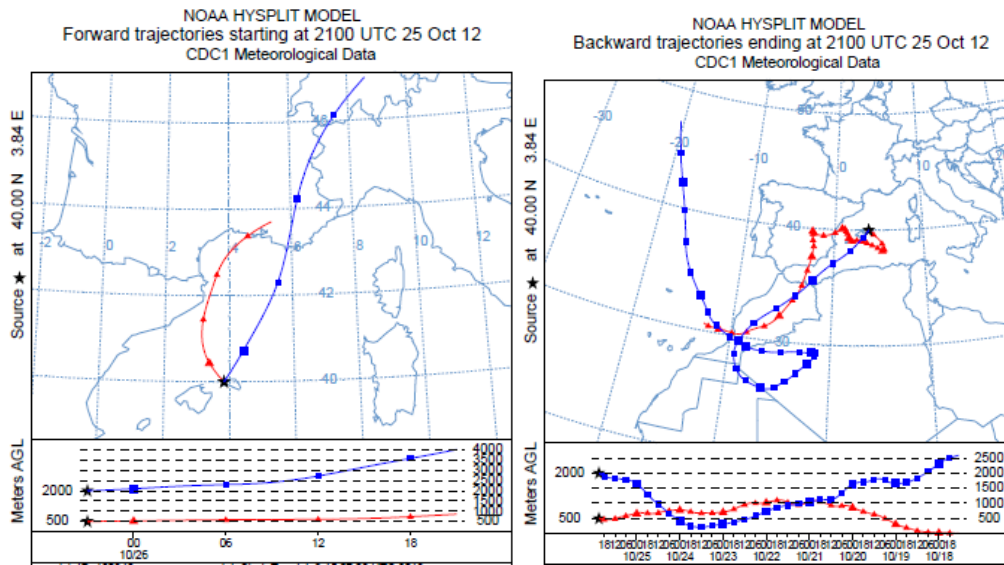
513

514

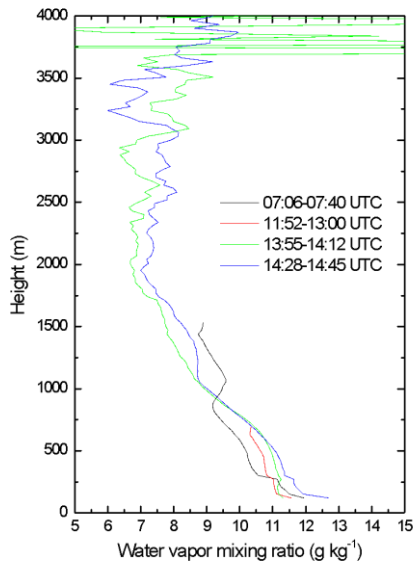
515 (c)

(d)

516



517



(e)

518 **Figure 3:** (a) Spatial distribution of 24 h-averaged GPS-derived IWV (mm) on 25 (top),
 519 and 26 (bottom) Oct. 2012. (b) Time evolution of the water vapor mixing ratio (g kg^{-1}) as
 520 measured by the ground-based lidar WALI in Menorca over the 48-h period from 00:00
 521 UTC, 25 Oct. 2012 to 00:00 UTC, 27 Oct. 2012. (c) 24-h forward trajectory analysis from
 522 HYSPLIT starting in Ciutadella (Menorca) at 21:00 UTC, 25 Oct. 2012 and ending at
 523 21:00 UTC, 26 Oct. 2012 and (d) 200-h back-trajectory analysis from HYSPLIT ending
 524 in Ciutadella (Menorca) at 21:00 UTC, 25 Oct. 2012. (e) Vertical profiles of the water
 525 vapor mixing ratio (g kg^{-1}) as measured by the ground-based lidar BASIL in
 526 Candillargues at different times on 26 Oct. 2012.

527 **3.3 Low-level dynamical processes**

528 Once the synoptic setting becomes favourable for heavy precipitation in the WMed, with
529 an upper-level trough slowly evolving eastward while deepening over the basin, the
530 mesoscale organization and the thermodynamic characteristic of the low-level flow
531 determines the occurrence, intensity and location of heavy precipitation. Most of the
532 severe rainfall events that occurred during the SOP1 field campaign can be connected
533 or at least interpreted in the framework of recent theoretical results concerning moist
534 orographic convection (Miglietta and Rotunno, 2014; Kirshbaum et al., 2018). However,
535 their in-depth analysis has revealed a greater complexity of real meteorological
536 situations, due to non-stationarity, to the complexity of the real 3D orography and vertical
537 profiles, and especially to the interaction among small-scale processes, which are not
538 entirely accounted for in controlled-environment numerical experiments. One of the
539 merits of HyMeX has been to provide evidence of the theoretical results and to enrich
540 our knowledge on genesis and evolution of convection in a complex topography
541 environment through a plethora of modelling simulations and tools, and advanced
542 instrument observations.

543 Being heavy orographic precipitation in stable and neutral atmospheric conditions
544 already investigated in past experiments (e.g., MAP-Mesoscale Alpine Programme,
545 Bougeault et al., 2001) and well understood, the focus of HyMeX was on the
546 development of quasi-stationary MCSs, well known responsible of recent HPE and floods
547 in the area (Nuissier et al., 2008; Buzzi et al., 2014; Romero et al., 2014 among others).
548 These systems are characterized by “back-building” processes that force the continuous
549 redevelopment of deep convective cells over the same area producing severe and
550 persistent rainfall (Schumacher and Johnson, 2005; Ducrocq et al., 2008; Duffourg et al.,
551 2018; Lee et al., 2018). The multicell MCSs resulting from this retrograde regeneration
552 assume a typical V-shaped pattern in radar and satellite images. In this context,
553 conditionally unstable marine flow directed towards the coastal mountainous regions and
554 extracting energy from the sea surface has been pointed out as a common feature of all
555 the events. However, different convection-triggering mechanisms have been identified
556 and highlighted.

557 **3.3.1 Convection-triggering mechanisms**

558 Low-level convergence over the sea can initiate convection even far from the coast and
559 usually it is produced by large-scale forcing. During IOP16 (Duffourg et al., 2016) the
560 cyclonic circulation around a shallow low-pressure system was responsible for low-level
561 convergence against the south-easterly flow, between Balearic Island and the Gulf of

562 Lion (Figure 4a). Lee et al. (2016) revealed the key role during IOP13 of an approaching
563 cold front in modifying the low-level circulation over the Tyrrhenian Sea, establishing
564 favourable dynamical conditions for convection initiation. Even for the IOP8, the low-level
565 convergence that first triggered convection south of the Iberian Peninsula was ascribed
566 to the large-scale setting (Röhner et al., 2016; Khodayar et al., 2015), even if orographic
567 effects were essential to enhance mesoscale uplift over land during the mature phase of
568 the convective system.

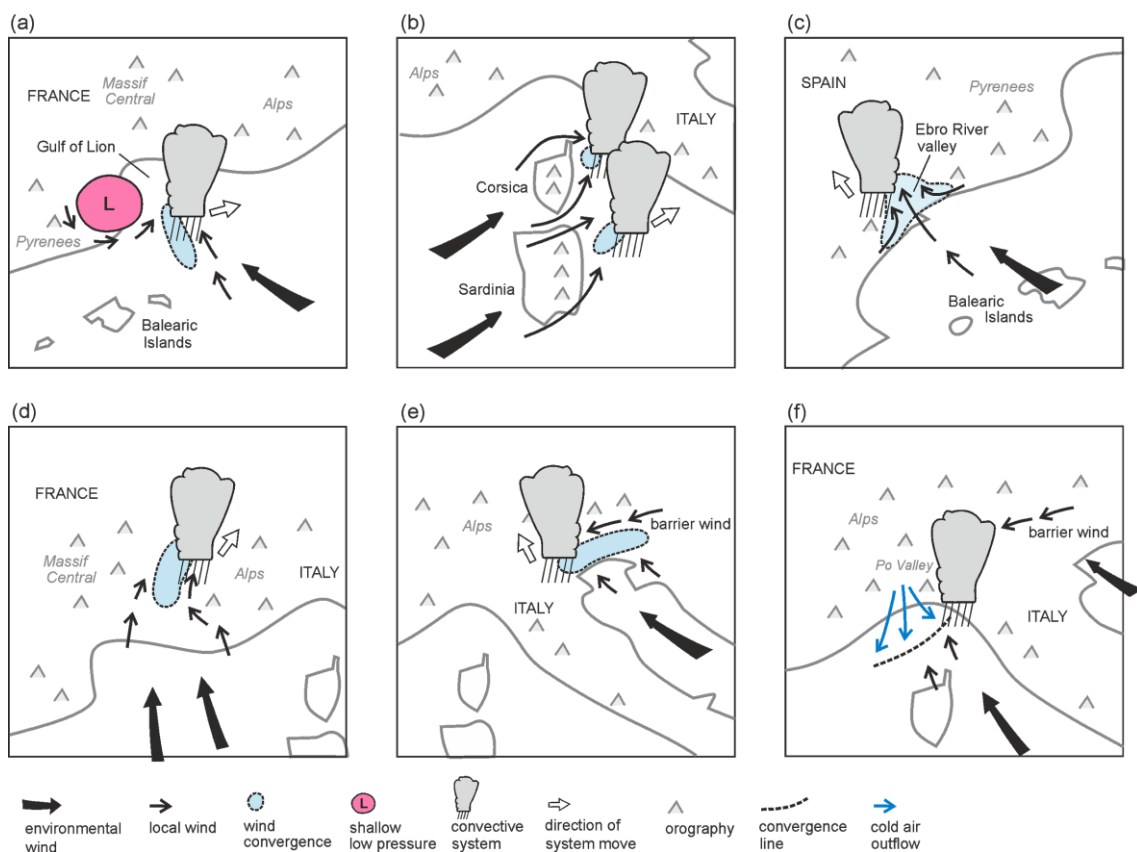
569 In fact, due to the peculiar topographic characteristics of the basin, in most of the events
570 it is the interaction with the orography that triggers and eventually maintains convection,
571 since it does provoke not only the direct lifting, but can also produce the convergence
572 required to initiate vertical motions. Several numerical experiments (Barthlott and
573 Davolio, 2016) clearly showed the effects of Corsica and Sardinia on the downstream
574 low-level wind as well as on temperature and moisture distribution. In particular, the
575 deflection of the westerly/south-westerly flow due to the complex orography of the islands
576 was identified as a key mechanism for the organization of heavy precipitation along the
577 western Italian coast, since it determined small-scale complex patterns of low-level
578 convergence over the sea in the lee of Corsica, where convection was triggered (Figure
579 4b). Moreover, the interaction between sea breezes and drainage winds induced by
580 mountainous islands like Corsica or Sardinia (Barthlott and Kirshbaum, 2013; Barthlott
581 et al., 2016) impacts on the development of deep convection both offshore and anchored
582 to topographic features. Also, the flow splitting around Corsica Island can be a key
583 mechanism producing a lee-side convergence line where a severe and stationary
584 convective system develops (Scheffknecht et al., 2016).

585 Interestingly, the study of Lee et al. (2017) clearly indicated that neither an offshore
586 convergence line nor the orographic uplift alone would have been enough to allow the
587 development of the intense MCS that affected the Ebro River valley during IOP 15
588 (Figure 4c). It was their interplay that produced deep convection, together with the
589 simultaneous presence of flow channelled by the local orography and converging with
590 the low-level marine inflow. This represents a clear example of the complex interaction
591 among processes that HyMeX was able to highlight.

592 Low-level convergence induced by the blocking effect of mountain chains on the
593 impinging flow is another frequent lifting mechanism upstream of the orography. Well
594 before the HyMeX SOP, it was demonstrated that flow blocking in front of Massif Central
595 and the enhanced convergence due to deviation of southerly flow around the Alps
596 (Figure 4d) (Ducrocq et al., 2008; Davolio et al., 2009), were responsible for several HPE

597 over southeastern France, affecting areas well upstream of the main orographic reliefs.
 598 SOP related studies identified a similar low-level flow characteristic, associated with
 599 heavy rainfall over northeastern Italy. In both the analysed events, occurred during
 600 IOP2b (Manzato et al., 2015; Miglietta et al., 2016) and IOP 18 (Davolio et al., 2016), the
 601 blocking of southerly low-level marine inflow in the form of a north-easterly barrier wind
 602 in front of the Alps, produced strong and localized convergence, favouring convection
 603 triggering (Figure 4e). Through additional modelling investigation of similar events in the
 604 past, this was recognised as a typical mechanism for deep convection (even supercell)
 605 development over the area.

606 The importance of orographic interaction has been revealed also for the development of
 607 lee-side convection. Pichelli et al. (2017) through several numerical simulations of IOP6
 608 illustrated the complex and delicate equilibrium between competing processes
 609 (orographically induced subsidence on the lee side and frontal uplift) that determined the
 610 evolution of a squall line over the Po Valley, in the lee side of a mountain range
 611 (Apennines) with respect of the main southerly flow feeding the precipitation.



612

613 **Figure 4:** Conceptual illustrations of key convection-triggering mechanisms in the north-
 614 western Mediterranean basin. Coast lines are depicted by grey solid lines.

615

616

3.3.2 Cold pools

617 The detailed observational and modelling analysis of IOP13 revealed that, as expected,
618 also the direct orographic uplift can trigger convection close to the coastal slopes.
619 However, thanks to detailed observations and modelling simulations of the precipitation
620 system and of the upstream environment, Duffourg et al. (2018) were able to provide a
621 thorough description of the mechanisms that maintained the MCS while slowly moving
622 offshore. In fact, the formation of an evaporative cold pool under the precipitating cells
623 generated down-valley flows that slowly shifted the location of the back building
624 convective cells from the mountain to the coast and over the sea.

625 In this regard, it was emphasized (Lee et al., 2018) that the moisture vertical distribution
626 in the lower troposphere can modulate the intensity of the cold pool and thus control
627 location and amount of heavy precipitation associated with the MCS. In several other
628 events, the leading edge of a cold pool, formed by evaporative cooling under the
629 precipitating cells, was able to trigger convection by lifting the impinging ambient low-
630 level flow. Ramis et al. (1994) already pointed out the convergence associated to a cold
631 pool boundary as a continued triggering convection mechanism in the WMed. As
632 suggested by idealized experiments of conditionally unstable flow over a mountain ridge
633 (Bresson et al., 2012; Miglietta and Rotunno, 2009), the stationarity of the MCS or its
634 upstream propagation away from the orographic barrier is determined by the intensity of
635 the ambient flow. In this context, the vertical structure of the lower troposphere, in terms
636 of moisture content and wind intensity, represents an important factor since it modulates
637 the evaporation potential and thus the formation and intensity of the cold pool.

638 However, the presence of cold and dense air acting as a virtual mountain with respect to
639 the impinging warm and moist flow can be due to different processes besides
640 evaporative cooling. In the analysis of IOP8, Bouin et al. (2017) identified cold and moist
641 air masses transported from the Gulf of Lion by the low-level jet. Despite their moisture
642 content, these air masses were cold and dense enough so that their accumulation on
643 the foothills of the relief contributed to initiating a cold pool. Once the MCS was triggered,
644 rain evaporation in the subsaturated mid-level layer resulted in downdraughts that further
645 intensified the cold pool, favouring the regeneration of the precipitation system. Finally,
646 investigation of heavy precipitation over Liguria in IOP16 as well as in previous dramatic
647 HPE, undertaken within the HyMeX framework, provided a clear picture of the
648 mechanisms responsible for recent and recurrent disastrous floods along the Ligurian
649 Sea coast. Several studies (Buzzi et al., 2014; Fiori et al., 2017 among others) pinpointed
650 the role of the cold air outflow from the Po Valley, across the Apennine gaps, which

651 propagate as a density current to the Ligurian Sea, where it determined a sharp
652 mesoscale convergence line (sketched in Figure 4f). Along such a convergence line, the
653 lifting of southerly moisture laden flow produced the onset of the severe convection.
654 Interestingly, the cold flow over the sea appeared to be induced by an easterly inflow into
655 the Po Valley from the Adriatic side, possibly due to a barrier wind effect over north-
656 eastern Alps as previously described. As observed in many other cases (e.g., Duffourg
657 et al., 2016) although the V-shape structure seems anchored over the sea, a few tens of
658 kilometres offshore, intense convective cells are continuously advected inland where HP
659 occurs. Finally, Duffourg et al. (2016) also highlighted an interesting feedback process
660 of convection to the environment that, through small-scale perturbations of the low-level
661 circulation around the cold pool, focussed and reinforced the local moisture convergence
662 feeding the convective updraft.

663 **3.4 Impacts of the land and the sea surfaces**

664 **3.4.1 Land conditions and feedback to the atmosphere**

665 Land conditions and feedbacks between the land surface and the atmosphere play a role
666 in determining the response of the Earth system to climate change, particularly in the
667 Mediterranean region, which is a transitional zone between dry and wet climates. Indeed,
668 enhanced land–atmosphere feedbacks are expected in a warming climate, and their
669 understanding and simulation are challenging, but fundamental to further improve our
670 knowledge about future climate and their interactions with the other components of the
671 climate system. Despite its relevance, the modelling of land-atmosphere feedback still
672 suffers for relevant uncertainty owing to inaccurate initialization, and/or model physics,
673 misspecified parameters, etc... Helgert and Khodayar (2020) showed that an
674 improvement of the soil-atmosphere interactions and subsequent HP modelling is
675 observed using an enhanced initialization with remote sensed 1 km SM information.
676 Khodayar and Helgert (2021) additionally investigated the response of the western
677 Mediterranean HP to extreme SM conditions showing that changes in the initial scenarios
678 impact the mean, but also the extremes of precipitation. Regional projections of
679 precipitation under the RCP4.5 and RCP8.5 scenario have shown to be considerably
680 modified when SM is used as a predictor (Hertig et al., 2018). Therefore, a better
681 knowledge and representation of soil conditions and evolution must be considered for
682 HP understanding and modelling.

683 **3.4.2 Air-sea interactions and coupling**

684 The Mediterranean Sea and the atmospheric boundary layer (ABL) continuously
685 exchange momentum, heat, and freshwater. These exchanges, related to the turbulent
686 fluxes, are controlled by the gradients of temperature, humidity, and velocity at the air-

687 sea interface. Rainaud et al. (2015) showed that although moderate air-sea fluxes were
688 observed during the HPEs of SOP1, large air-sea exchanges in the Gulf of Lion and the
689 Balearic, Ligurian and Tyrrhenian Seas can be correlated to the occurrence of a HPE.
690 The SST strongly influences the low-level flow stability and dynamics through heating,
691 moistening and downward momentum mixing (Stocchi and Davolio, 2017; Meroni et al.,
692 2018a). SST is indeed a key parameter for evaporation (Figure 5a) and its influence on
693 HPEs in terms of convection triggering, intensity, and location, has been extensively
694 investigated with several numerical studies (e.g., Strajnar et al., 2019; Senatore et al.,
695 2020b, for some of the most recent). Generally, these studies highlight that the SST
696 values strongly and directly modify the low-level atmospheric stability, which first impact
697 the intensity of convection and precipitation, with the most intense rainfall associated
698 with warmer sea surface. The location and stationarity of heavy precipitating systems
699 are also modified, with an acceleration of the low-level wind velocity over warmer sea,
700 but also by the fine-scale SST horizontal patterns with eddies and marked fronts in the
701 Mediterranean (as explicitly simulated in the coupled forecast of Rainaud et al. (2017)
702 for IOP16a shown in Figure 5a) that can significantly change the flow dynamics
703 interacting with orography (Davolio et al., 2017) or displace the moisture convergence at
704 sea (Rainaud et al., 2017; Meroni et al., 2018a).

705 During intense meteorological events in the Mediterranean such as HPEs, significant
706 modifications of the ocean mixed layer (OML) can occur, even on short timescales of
707 only several hours (Lebeaupin Brossier et al., 2014), and can significantly impact the
708 exchanges with the ABL. Berthou et al. (2016) showed that IOP16a was likely sensitive
709 to SST changes upstream related to OML changes and sub-monthly air-sea coupling.
710 The ocean vertical stratification is also a characteristic which has to be accounted for, as
711 sea surface cooling during HPEs is largely controlled by the entrainment of deeper and
712 colder water in the OML. The study of Meroni et al. (2018b) using coupled experiments
713 with idealized ocean conditions highlights that the cooling is more pronounced with a
714 shallow, strongly stratified OML, leading to lower air-sea fluxes, less air instability and
715 finally a reduction of the total amount of simulated precipitation.

716 The use of ocean-atmosphere coupled systems enables us to consider the ocean 3D
717 structure and its interactive and consistent evolution. Such modeling systems were
718 specifically developed in the framework of HyMeX to improve the realism of weather
719 forecasts for sea surface and atmospheric low levels, and innovatively evaluated thanks
720 to the multi-compartments' observational dataset. For IOP16a, Rainaud et al. (2017)
721 showed that, due to mixing and heat loss, the progressively lower SST in the coupled
722 model induces lower heat fluxes (-10% to -20% of evaporation), local differences in the

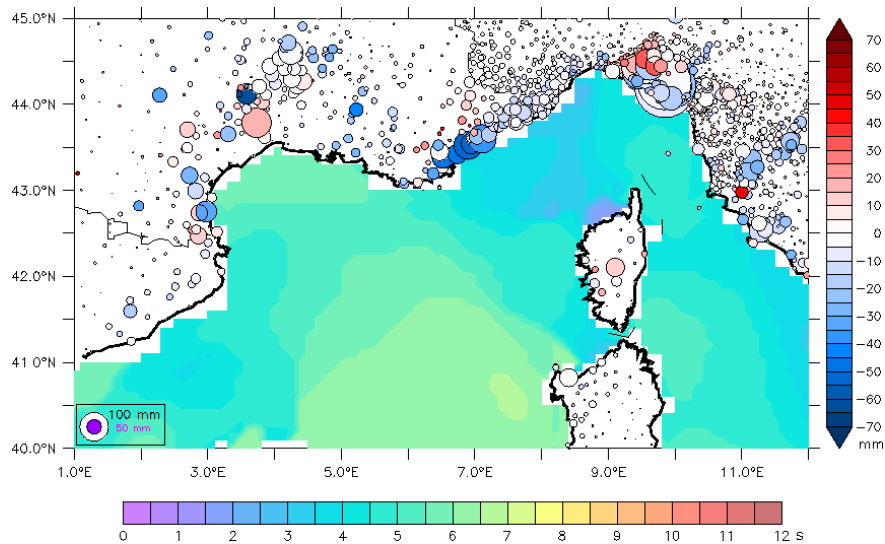


Figure 5: (a) Daily mean SST (colours, °C), 10m-wind (arrows, m s^{-1}) and surface evaporation (green contours for values above 600 kg m^{-2}) for 26 Oct. 2012 (IOP16a) from the AROME-NEMO WMED coupled experiment (CPLOA) of Rainaud et al. (2017). (b) Peak period of waves (color, s) at 00:00 UTC, 26 Oct. 2012 considering in Thévenot et al. (2016) and bias modification (circles, mm) for 24h-rainfall accumulation against rain-gauges data, comparing MESO-NH simulations with (WAM) and without (NOWAV) sea state impact (blue for an improvement in WAM). The size of the circles indicates the NOWAV bias (absolute value, in mm).

733

734

735

3.5 Microphysics

736 Many advances in the understanding and knowledge of cloud composition and
 737 microphysical processes in Mediterranean convective systems were attained in the
 738 framework of HyMeX, thanks to the large number of observations used in process,
 739 modeling and/or data assimilation studies.

740 Among them, a large number of available disdrometers and MRRs were used to improve
 741 the quality of observations (Raupach and Berne, 2016 and Adirosi et al., 2016) and the
 742 characterization of the raindrop's PSD (Adirosi et al., 2014, Adirosi et al., 2015, Schleiss
 743 and Smith, 2015), including its very small-scale variability (Gires et al., 2015).

744 Based on rain gauge observations over a long period encompassing the HyMeX
 745 experiment, Molinié et al. (2012) studied the rainfall regime in a mountainous
 746 Mediterranean region, in southeastern France. They found that rainfall intermittency,
 747 both at the monthly and daily scales, is well correlated to the rain gauge altitude, which
 748 is also linked to rainfall intensity. Zwiebel et al. (2015) and Hachani et al. (2017) also
 749 found that several factors (altitude, season, weather type, among others) influence both

750 the rainfall characteristics at the ground and the relationship between rainfall rate and
751 the reflectivity factor.

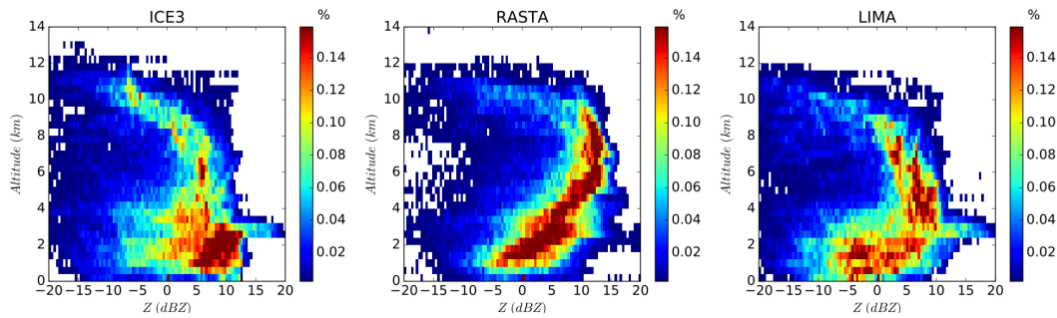
752 Other studies focused on the use of radar data to investigate cloud composition. Grazioli
753 et al. (2015) proposed a hydrometeor classification algorithm using an X-Band radar
754 (deployed in Ardèche during HyMeX SOP1). Ribaud et al. (2015) also developed a
755 hydrometeor classification algorithm using dual-polarimetric radars and produced 3D
756 hydrometeor fields when several radars were available. Using this classification, they
757 also identified a link between cloud characteristics and lightning propagation (Ribaud et
758 al., 2016).

759 HyMeX microphysical observations have also led to improvements in model physics and
760 parameterizations. Fresnay et al. (2012) first demonstrated the sensitivity of
761 Mediterranean HPEs simulations to the cloud parameterization. Using several
762 observations from HyMeX SOP1, Taufour et al. (2018) showed that the 2-moment
763 scheme LIMA (Vié et al., 2016) provides a more realistic cloud representation than the
764 1-moment scheme ICE3. This is shown in Figure 6, which presents the distribution of the
765 simulated and observed RASTA reflectivities, sorted by altitude. Data from IOPs 6 and
766 16 were combined and classified in bins of altitude and reflectivity, and the number of
767 events in each category was normalized by the total number of data points to provide
768 the colored frequency. The shape of the reflectivity distribution is better represented
769 by LIMA than ICE3, especially in the melting region. Furthermore, Taufour et al. (2018)
770 proposed a revision of the scheme LIMA based on the disdrometer rain PSD
771 observations.

772 The aerosol-cloud interactions were also found to have a strong impact on convective
773 systems and rainfall characteristics (Kagkara et al., 2020), and the best simulation results
774 with the 2-moment scheme LIMA are obtained when using a realistic aerosol population
775 from the MACC analyses validated against ATR42 observations (Taufour et al., 2018).

776 Eventually, some studies prepared the future assimilation of cloud data. Augros (2015)
777 implemented the assimilation of dual-polarization radar data in the French operational
778 AROME model. Borderies et al. (2019a, 2019b) proposed a method to assimilate
779 airborne RASTA reflectivities and Doppler winds, meanwhile releasing an improved
780 version of the RASTA simulator for use in mesoscale models.

781



782

783 **Figure 6:** Distribution of simulated (left : ICE3, right : LIMA) and observed (center)
 784 RASTA reflectivities sorted by temperature, merging data from IOPs 6 and 16a (From
 785 Taufour et al. 2018).

786

787 4. Improving Heavy precipitation modelling across scales

788 4.1 Increasing model resolution simulations

789 Idealized simulations of deep moist convection at kilometric scales (grid spacing: 4 km,
 790 2 km, 1 km and 500 m) showed that the accumulated rainfall and corresponding surface
 791 area, as well as the area covered by the updrafts, increase with increasing resolution. At
 792 4 km horizontal resolution, deep convection is under-resolved, and differences are larger
 793 between 1 km and 500 m horizontal resolution simulations than between 2 and 1 km,
 794 suggesting the beginning of convergence at 500 m (Verrelle et al., 2014). Bassi (2014)
 795 analysed several IOPs over LT target area performing numerical simulations at different
 796 grid-spacings between 3 and 1 km, and with different resolutions of the orography
 797 representation, showing that both aspects equally contributed to improve the quantitative
 798 precipitation forecast (QPF). In fact, the higher model resolution allowed a better
 799 description of the structure, vertical motions, and dynamical mechanisms of the
 800 convective system, whereas accurate orography was required to correctly simulate the
 801 propagation of the density current along the Apennine slopes, and thus the precise
 802 location of the convergence line that triggered the MCS. In terms of microphysics
 803 parameters, discrepancies between models and observations could be attributed to the
 804 implementation of one-moment microphysics scheme and to the coarse resolutions,
 805 hence, there is a need for grid spacing finer than 2.5 km (Augros et al., 2015).

806 The increase in horizontal resolution is therefore a great improvement but it additionally
 807 poses challenges for the model physics since some parameterization schemes may
 808 become inappropriate. This is the case, for example, of the turbulence parameterization
 809 in the “grey zone” between 1 km and 100 m horizontal grid spacing (Wyngaard and Coté,

810 1971), or of one-moment microphysical schemes where the overestimation of
811 reflectivities at high altitude due to graupel is a known limitation (Varble et al., 2011).

812 Hectometric-scale simulations of a Mediterranean HP event at 150 m by Nuissier et al.
813 (2020) were able to capture features regarding convective organization within the
814 converging low-level flow, which are out of range of models with kilometric horizontal
815 resolutions. However, the comparison of the large-eddy simulation (LES) with a
816 reference simulation performed with a 450 m grid spacing in the heart of the so-called
817 “grey zone” of turbulence modelling shows that the increase in resolution does not
818 significantly reduce deficiencies of the simulation, being this fact more related to an issue
819 of initial and lateral boundary conditions.

820 **4.2 New generation of high-resolution convection permitting simulations** 821 **and improvement of RCMs**

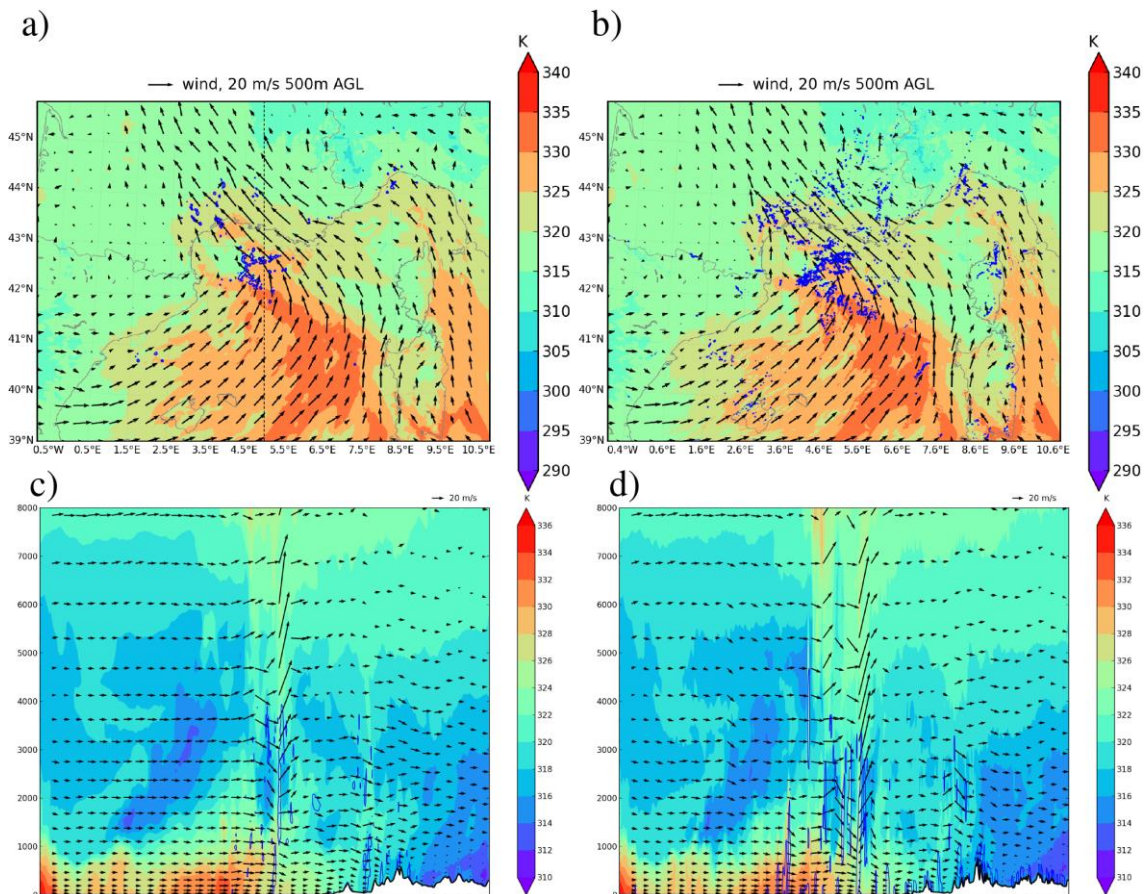
822 One of the most remarkable advances in the last years with significant implications for
823 HP simulation has been the development of the new generation of high-resolution
824 convection-permitting models (CPMs). This development has been extensively fostered
825 and exploited in HyMeX related activities and studies and represented one of the main
826 innovations contributing to advance knowledge in HP occurrence. Kilometric grid spacing
827 has become achievable with the increasing availability of computational resources. As
828 the horizontal resolution approaches 1 km, parameterization of deep convection is no
829 longer needed since much of the convective motion is explicitly resolved. It has been
830 demonstrated that the reduction of the grid spacing leads to a weaker overestimation in
831 height and size of the convective cells (Caine et al., 2013), together with a more accurate
832 representation of the timing and location of convection (Clark et al., 2016).

833 The benefit of higher horizontal resolution of CPMs can also propagate along the
834 forecasting chain to hydrological predictions. Simulating the catastrophic Liguria floods
835 of 2011, Davolio et al. (2015) demonstrated that the finer grid resolution resulted in better
836 QPF because of a more accurate description of the MCS and of its interaction with the
837 orography, and this improvement was confirmed also in terms of discharge forecasts.

838 In a seamless weather-climate multi-model intercomparison, Khodayar et al. (2016a)
839 showed that despite differences in their representation of a HPE, CPMs represented
840 more accurately the short-intense convective events, whereas the convection-
841 parameterized models produce many weak and long-lasting events and RCMs produce
842 notably lower precipitation amounts and hourly intensities. Figure 7 shows an example
843 of how finer resolution simulations better represent convergence over the sea, where

844 warm and moist air is transported by a low-level jet towards the French coast. The higher
845 resolution enhances the humidity convergence areas over the sea, which appear located
846 further upstream, as well as the associated triggering of convection. Furthermore, the
847 added value of convection-permitting with respect to RCMs has also been demonstrated
848 in the north-western Mediterranean basin (e.g., Berthou et al., 2018; Coppola et al.,
849 2018; Fumière et al., 2019). Berthou et al. (2018) showed that convection permitting
850 RCM simulations (about 2.5 km grid spacing) better represented HPE in southern France
851 in terms of daily precipitation than their convection-parameterized counterparts (about
852 12.5 km grid spacing). It was also shown the added value for the simulation of hourly
853 rainfall over the United Kingdom, Switzerland, and Germany. Coppola et al. (2018), in a
854 multi-model study, proved the ability of high-resolution CP-RCMs to reproduce three
855 events of HP, one in summer over Austria, one in fall associated with a major Foehn
856 event over the Swiss Alps and another intense fall event along the Mediterranean coast.
857 In a dedicated study of Mediterranean HPEs in fall on an hourly time scale, Fumiere et
858 al. (2019) demonstrated that high resolution allows, (a) the improved representation of
859 the spatial pattern of fall precipitation climatology, (b) the improvement of the localization
860 and intensity of extreme rainfall on a daily and hourly time scales, and (c) the ability to
861 simulate intense rainfall on lowlands.

862



863

864 **Figure 7:** IOP16: 0930 UTC, 26 Oct. 2012. Horizontal cross sections at 500m AGL and
 865 vertical cross sections along a South-North line (shown in a) of equivalent potential
 866 temperature (K, in colour scale), and wind vectors (m s^{-1} , black arrows) for 2-km (left
 867 panels) and 500-m (right panels) resolution runs. The blue lines represent the humidity
 868 convergence ($-0.1 \text{ kg s}^{-1} \text{ m}^{-3}$ for vertical cross sections, and $-0.02 \text{ kg s}^{-1} \text{ m}^{-2}$ integrated
 869 value over the layer between the ground and 3000 meters for horizontal cross sections).
 870

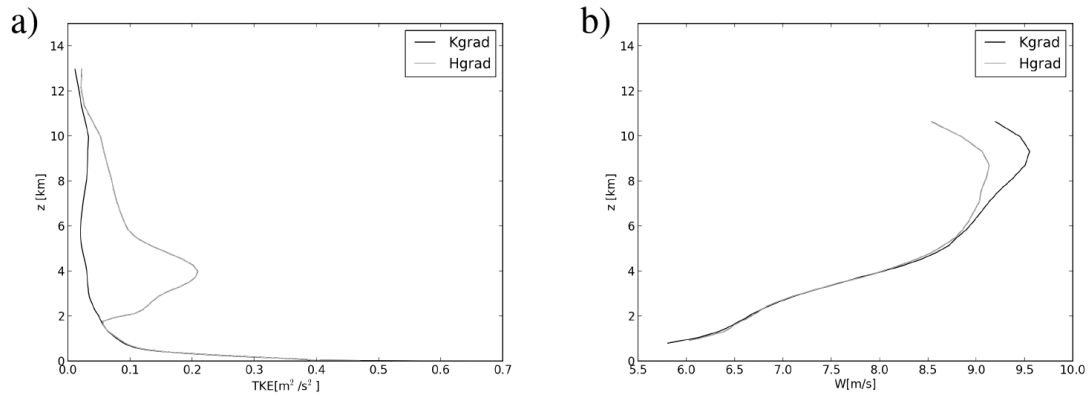
871 4.2 Improvement of parameterization schemes

872 Recent studies have shown that the simulation of convective systems is very sensitive
 873 to model parameterizations. For the IOP16a, Thévenot et al. (2015) showed that taking
 874 sea state into account in the turbulent air-sea exchanges can modify the low-level
 875 dynamics of the atmosphere and the precipitation location. However, the relationship of
 876 Oost et al. (2002) used in this study to compute the roughness length is known to
 877 overestimate the turbulent fluxes in strong wind regimes. New formulation of sea surface
 878 turbulent fluxes parameterization is under development and currently tested to better
 879 represent the wind-sea (i.e., the younger waves locally generated by wind) impact and
 880 related variability. The preliminary results when applied to HPE forecasts confirm the

881 significant slow-down of the upstream low-level flow with displacement of convergence
882 over the sea and show minor changes in the heat and moisture fluxes (Sauvage et al.,
883 2020). Further developments are planned concerning sea surface fluxes computation,
884 including notably the impact of sea spray on moisture and of the swell (i.e., the oldest
885 non-local waves).

886 In Rainaud et al. (2015), a change in the SST or the coupling of atmospheric and oceanic
887 models is found to have a large impact on the simulated precipitation amount over land.
888 Martinet et al. (2017) investigated the sensitivity of simulated HP at a sub-kilometric scale
889 (500 m) to the turbulence parameterization (i.e., Deardorff or Bougeault-Lacarrère)
890 showing that the simulated environment and convective processes are highly sensitive
891 to the formulation of the mixing-length. Convective systems are more intense in
892 association to larger moisture advection, higher hydrometeor contents and marked low-
893 level cold pools with weaker mixing lengths, since in this case the subgrid TKE is weaker,
894 and winds are increased to balance this effect.

895 Moreover, Verrelle et al. (2014) found insufficient turbulent mixing inside convective
896 clouds, more pronounced at kilometer resolution with weak thermal production,
897 underlying a lack of entrainment in convective clouds at intermediate range (between
898 500 m and 2 km horizontal resolution). By using LES of deep convection, Verrelle et al.
899 (2017) and Strauss et al. (2019) showed that the commonly used eddy-diffusivity
900 turbulence scheme (K-gradient formulation) underestimated the thermal production of
901 subgrid TKE and did not enable the nonlocal turbulence due to counter-gradient
902 structures to be reproduced. These two studies also found that the approach proposed
903 by Moeng (2010), parameterizing the subgrid vertical thermodynamical fluxes in terms
904 of horizontal gradients of resolved variables (H-gradient approach), reproduced these
905 characteristics, and limited the overestimation of vertical velocity. This new approach has
906 also been assessed using Meso-NH simulations at kilometer-scale resolutions for real
907 cases of deep convection on two HyMeX IOPs (IOP6 and IOP16a) (Ricard et al., 2021).
908 The new scheme enhances the subgrid thermal production of turbulence with a better
909 representation of counter-gradient areas and reduces the vertical velocity inside the
910 clouds (Figure 8). The enhanced turbulent mixing modifies the entrainment and
911 detrainment rates and produces more developed anvils with increased values of ice and
912 snow, which are more realistic. It also affects the cold pool under the convective cells.



913

914 **Figure 8:** Mean vertical profiles inside the clouds of (a) subgrid TKE ($\text{m}^2 \text{s}^{-2}$) and (b)
 915 vertical velocity (m s^{-1}) during IOP16 (between 00:00 UTC, 26 Oct and 00:00 UTC, 27
 916 Oct. 2012) for 2-km horizontal resolution Meso-NH simulations using K-gradient
 917 formulation (black line) and H-gradient formulation (grey line) for the vertical turbulent
 918 fluxes of heat and moisture.

919

920 4.3 Data Assimilation

921 One of the HyMeX goals was to improve or develop research- as well as operational-
 922 oriented atmospheric data assimilation systems and methods. Emphasis has been put
 923 on progress in the processing of observations currently available in data assimilation
 924 systems and on the assimilation of new observation types, especially aimed at improving
 925 the prediction of HP.

926 Campins and Navascués (2016) evaluated the impact of targeted observations on
 927 HIRLAM forecasts during HyMeX-SOP1 showing that the assimilation of radiosoundings
 928 and Advanced TIROS Operational Vertical Sounder (ATOVS) satellite observations
 929 clearly improve the first-guess quality over land and sea sensitive areas respectively. A
 930 real-time implementation of the HyMeX-dedicated version of the Météo-France AROME
 931 NWP system covering the whole WMed ran from 01 September 2012 to 15 March 2013
 932 (Fourrié et al., 2015). The same system was used to perform an extensive reanalysis of
 933 SOP1 exploiting observations from research instruments deployed during the campaign
 934 in addition to the operational observations assimilated in real-time (Fourrié et al., 2019).
 935 For that, processing of observations and systematic comparisons between observations
 936 and AROME short-range forecasts were carried out for: i) ground-based Lidar water
 937 vapour observations in Candillargues (BASIL) and at Menorca (WALI), ii) airborne Lidar
 938 LEANDRE II water vapour observations along the SAFIRE/ATR42 flight tracks, iii) high-
 939 resolution radiosoundings from operational sites in France and Spain and HyMeX -

940 dedicated radiosoundings launched during SOP1 over France and Italy, iv) dropsondes
941 observations and in-situ observations from the three research aircrafts, v) reprocessed
942 wind profiler observations, vi) reprocessed delays from more than 1000 GPS receivers
943 over France, Spain, Portugal and Italy, vi) radar data from five AEMET operational radars
944 over Spain, vii) additional SST observations from ship and Argo floats. The skill scores
945 showed a better performance for the forecasts starting from the re-analysis than those
946 starting from the real-time AROME-WMED analysis. AAdditional benefits were identified
947 such as the detection of a secondary cyclone producing severe weather in Menorca
948 during IOP 18 (Carrió et al. 2020).

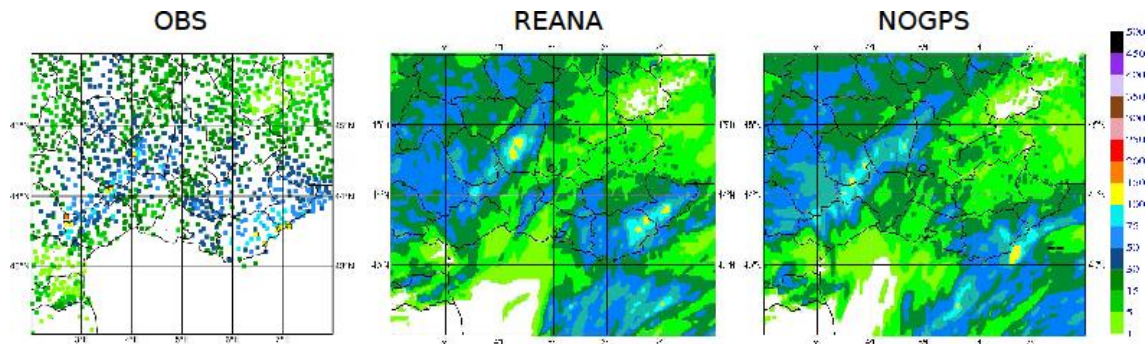
949 Data denial experiments, for which one of the above-listed datasets was removed from
950 the reanalysis at a time, clearly showed the benefit of assimilating the reprocessed GPS
951 ground-based zenithal total delays as shown in Figure 9.

952 This result was confirmed in other studies. Lindskog et al. (2017) demonstrated the
953 benefits of GPS assimilation to the forecast quality. Bastin et al. (2019) pointed out that
954 the general overestimation of low values of IWV in RCM models over Europe was
955 reduced when using a nudging technique to assimilate IWV information. Caldas-Alvarez
956 and Khodayar (2020) and Caldas-Alvarez et al. (2021) highlighted the positive impact
957 exerted by moisture corrections on precipitating convection and the chain of processes
958 leading to it across scales. Furthermore, the implementation of nudging methodologies
959 to exploit non-conventional observations, such as rainfall estimates from remote sensing,
960 provided positive results in applications to both nowcasting and short-term meteo-
961 hydrological forecasting (Davolio et al., 2017; Poletti et al., 2019).

962 The potential of several new types of observations within cloudy and precipitating
963 systems have also been investigated. As a first step towards assimilation, “observation
964 operators”, which consist in simulating observations from model outputs, have been
965 developed. In the framework of HyMeX, a dual-polarization weather radar simulator has
966 been developed in the post-processing part of the Meso-NH mesoscale model (Augros
967 et al., 2015). An observation operator for the airborne Rasta reflectivity observations has
968 also been developed (Borderies et al., 2019a). The impact of the assimilation of RASTA
969 data on AROME-WMED analyses and forecasts has been assessed. IOP7a results
970 indicated an improvement in the predicted wind at short-term ranges (2 and 3 hours) and
971 in the 12-hour precipitation forecasts. Over a longer cycled period, a slightly positive
972 improvement in the 6-, 9- and 12-hour precipitation forecasts of heavy rainfall has been
973 demonstrated (Borderies et al., 2019a). The assimilation of RASTA reflectivity data in
974 AROME-WMED over the whole SOP1 period resulted in an improvement of rainfall
975 forecasts even larger when wind was jointly assimilated (Borderies et al., 2019b).

976 Finally, HyMeX has fostered the inception of a collaboration between CNRM (France)
977 and CNR-ISAC (Italy) concerning the assimilation of radar data. The assimilation of radar
978 reflectivity factor together with lightning, showed a significant and positive impact on the
979 short-term precipitation forecasts (Federico et al., 2019).

980



981

982 **Figure 9:** 24 hour accumulated precipitation (mm/24hr) between 06:00 UTC, 26 Oct. and
983 06:00 UTC, 27 Oct. 2012 over southern France (zoom over Cévennes area);
984 observations (left panel), REANA (middle panel) and NOGPS (right panel) simulations.

985

986 **4.4 Predictability and ensemble forecasts**

987 Despite advances in numerical modelling and data assimilation, the prediction of HP and
988 related floods remains challenging because predictability of intense convective systems
989 is limited, and user expectations are very high given the impact of HPEs. Ensemble
990 prediction techniques can provide solutions through the elaboration of probabilistic HPE
991 warnings. Until the 2010s, regional ensemble prediction systems were mainly limited by
992 the large computational costs of increasing the members resolution and the ensemble
993 size. Ensemble forecasts become even more useful when post-processing techniques
994 are applied to the precipitation fields, using statistical methods such as regression or
995 analogues (Diomedede et al., 2014), with some difficulties due to the geographically
996 complex forecast error structures of Mediterranean precipitation, and to the need of
997 preparing very long reforecast datasets in order to adequately sample the statistical
998 behaviour of HPEs.

999 With the availability of more powerful computational resources, operational regional
1000 models started to reach the kilometeric resolution leading to physically more realistic
1001 convection-permitting ensemble prediction systems (CPEPS). Studies of HPE events
1002 (Nuissier et al., 2016) have shown the added value of CPEPS over deterministic
1003 approaches or lower resolution ensembles. The enhanced exchange of validation

1004 datasets during HyMeX facilitated the objective verification of this kind of result in several
1005 ensemble studies such as Roux et al. (2019).

1006 Several studies in the framework of HyMeX have demonstrated that, besides sensitivity
1007 to synoptic scale forcing represented by lateral boundary condition (LBC) perturbations,
1008 CPEPS systems were sensitive to multiple error sources, which had to be sampled as
1009 specific perturbation in the parameterization schemes. Some sensitivity of ensemble
1010 spread to the model physics (turbulence and microphysics schemes) was demonstrated
1011 in Hally et al. (2014), who used the HyMeX IOP6 and IOP7a forecast and observation
1012 dataset to show that LBC perturbations cannot be neglected, and that the relative
1013 importance of LBC and physics uncertainties is case-dependent, with physics
1014 uncertainty being more significant during weakly forced convective events. Vié et al.
1015 (2012) explored the impact of microphysical processes on CPEPS spread and found a
1016 relationship between precipitation evaporation and the uncertainty of cold pool formation,
1017 which can be relevant to predict the correct location of HPEs. Bouttier et al. (2015) found
1018 a beneficial impact of randomly perturbing surface fields such as SST or soil moisture:
1019 the high density of HyMeX SOP1 data gave statistical significance to these results,
1020 because the objective verification of ensembles at high resolution requires large
1021 observational datasets.

1022 Besides developing physics perturbation techniques, other ensemble approaches were
1023 tested in HyMeX case studies, based on different models or parameterization schemes.
1024 This multiphysics or multi-model technique was shown to be relevant to HPE events in
1025 several studies, such as Davolio et al. (2013), Hally et al. (2015), Ravazzani et al. (2016).
1026 Compared to other sources of uncertainty, the maximum impact of physics, multiphysics
1027 or surface perturbations tends to be observed at forecast ranges between a few hours
1028 and about one day, after which the CPEPS behaviour is usually dominated by the LBCs.
1029

1030 The specification of the ensemble LBCs can be optimized in terms of the HPE forecasts:
1031 Nuissier et al. (2012) showed that LBC member selection from a global ensemble, using
1032 a clustering technique, improves over a random selection. Marsigli et al. (2014)
1033 demonstrated that direct nesting into the ECMWF ensemble, instead of using an
1034 intermediate model, is beneficial despite the large resolution jump between the global
1035 and CP ensemble.

1036 Initial condition perturbations using ensemble data assimilation systems were studied in
1037 Vié et al. (2012) and Bouttier et al. (2016). They found that initial condition perturbations
1038 are critical to achieve a correct CPEPS ensemble spread, typically during the first twelve

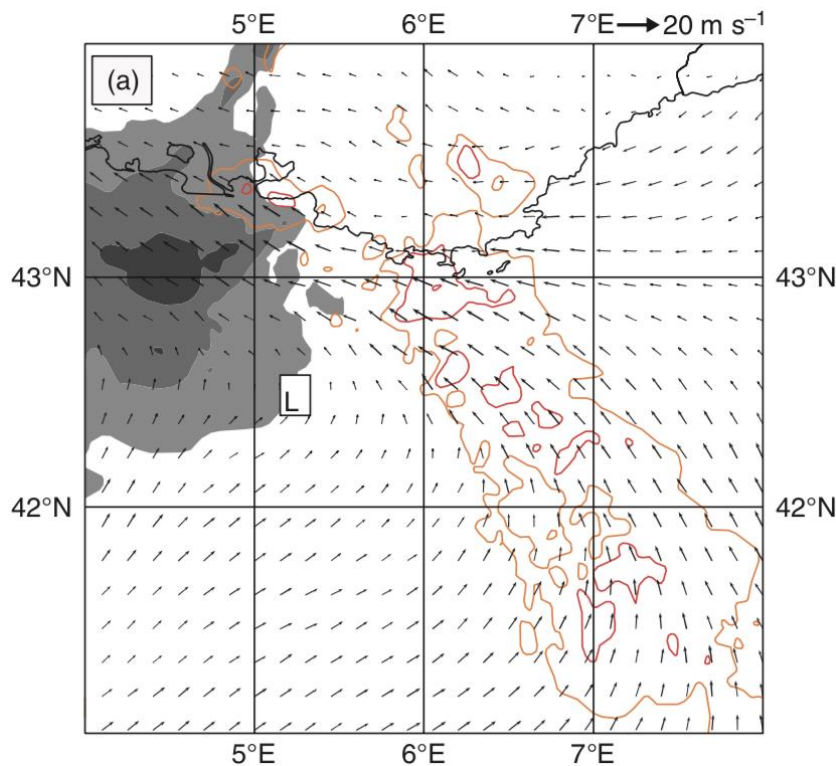
1039 hours of prediction, after which other perturbation sources (LBCs, surface and stochastic
1040 model perturbations) tend to dominate.

1041 Verification of ensemble forecasts of HPEs can be overtaken using probabilistic scores,
1042 It greatly benefits from the large amount of observations available during the SOPs.
1043 Ensemble predictions can also be evaluated by their ability to drive ensembles of
1044 hydrological runoff models. Indeed, it was confirmed during HyMeX that although
1045 hydrological models suffer for their own uncertainties (Edouard et al., 2018), precipitation
1046 forecast errors are the main sources of uncertainty for flood prediction. Many studies
1047 dealing with CPEPS also exploited precipitation forecasts to drive flood prediction
1048 systems. Among others, Roux et al. (2019) pointed out that enhancing the spread of HPE
1049 precipitation forecasts tends to help flood warnings by improving the detection of extreme
1050 HPE scenarios.

1051 An emerging application of CPEPS forecasts consists in investigating the physical
1052 mechanisms that drive HPE events (and, possibly, the reasons behind forecast failures),
1053 as exemplified in the USA by Nielsen and Schumacher (2016). In the HyMeX framework,
1054 beside the above-mentioned studies on physical perturbations, importance of
1055 orographically driven low-level flows was confirmed using CPEPS in Hally et al. (2014)
1056 and Nuissier et al. (2016). Figure 10 shows an example for the IOP16 case.

1057

1058



1059

1060

1061 **Figure 10:** Lowest quartile of the mean sea-level pressure (shading), mean 10m wind
1062 (arrows) and mean moisture flux at 925hPa (solid lines: 80 and 100 g m s⁻²) valid at 12:00
1063 UTC, 26 Oct. 2012 for the AROME-EPS ensemble. (credits: Nuissier et al., 2016)

1064

1065

1066 **5. Discussion**

1067 The spatial complexity of the Mediterranean region, the intricacy of the dynamical and
1068 physical processes involved including the multiple interactions across scales, as well as
1069 the technical and observational limitations in the past have made HP understanding and
1070 modelling in the Mediterranean region a very challenging issue. To try to advance in this
1071 direction the Hydrological Cycle in the Mediterranean Experiment (HyMeX, 2010-2020)
1072 has put a major effort in investigating the predictability and evolution of extreme weather
1073 events. Within this framework and profiting from the state-of-the-art observational
1074 datasets and modelling capabilities lately available and developed within the
1075 programme, important achievements towards improved understanding of the
1076 mechanisms leading to HP in the WMed have been accomplished. In this paper we
1077 review the main advances and lessons learned during HyMeX, including results emerged
1078 from cross-disciplinary studies.

1079

1080 The unprecedented richness of observations and numerical experiments during HyMeX
1081 led to major achievements and the identification of primary needs for an improved
1082 understanding and predictability of HPE. Our better comprehension of the moist
1083 convergence role on MCS initiation over the sea, the first-time airborne observations of
1084 WCB, the high space-time resolution measurements of the 3-D fields of water vapour, or
1085 the testing of new convection-permitting ensembles, which provided new insights on
1086 HPE predictability and of forecast error sources, among others illustrate the main
1087 accomplishments achieved during HyMeX. Parallel to this, observational, modelling and
1088 knowledge gaps have been identified clearly indicating the needs for future applications.
1089 Sensitivity to soils and sea surface conditions with impacts on high-resolution forecasts
1090 pointed out the need to build and/or improve high-resolution coupled systems able to
1091 represent the full evolution of the soil and ocean conditions. The need of a higher number
1092 of observations, for example collected over the sea, thermodynamic profile
1093 measurements and wind on a high space-time resolution would have a major impact on
1094 forecasting capabilities, through the initialization of modelling systems, data assimilation
1095 and the definition of improved parameterization schemes for turbulence and convection.

1096 Also, open questions remain regarding access to large samples of HPE reforecasts, the
1097 representation of model error processes specific to HPE systems and persisting
1098 shortcomings in the real-time prediction of extreme precipitation events for flood
1099 warnings, among others. Furthermore, coordinated research efforts will be needed to
1100 address topics of multi-scale interactions, from large-scale dynamics to microphysical
1101 processes.

1102

1103 Along with the achievements and demands, the continuous collaboration between
1104 scientific communities, e.g., oceanographers and meteorologists, and among scientific
1105 teams (ST) has been a priority and a success of the project. In fact coordinated efforts,
1106 in particular with the ST-lightning (Lightning and atmospheric electricity), ST-TIP
1107 (Towards integrated prediction of heavy precipitation, flash-floods and impacts), ST-ffv
1108 (Flash-floods and social vulnerabilities), and ST-medcyclones (Mediterranean
1109 Cyclones), through the development and use of common observation and modelling
1110 tools, and by sharing results and expertise, helped each other towards common goals.
1111 As illustration, aiming at a better understanding of processes leading to flash floods, as
1112 well as at their accurate modelling and forecasting, the ST-ffv actively contributed to the
1113 improvement of heavy rainfall prediction. Several recent multidisciplinary studies
1114 investigated the possibility to have an integrated modelling approach from heavy rainfall
1115 forecasting, to discharge prediction, to social impact. Methodologies of postflood field
1116 surveys based on interdisciplinary collaborations between hydrologists and social
1117 scientists have been proposed (Ruin et al., 2014; Borga et al., 2019). For instance,
1118 Papagiannaki et al. (2017) investigated the link between HP and impacts on the flash
1119 flood that occurred in October 2015 in Attica. The survey responses provided insights
1120 into risk perception and behavioral reactions relative to the space-time distribution of
1121 rainfall. Different possibilities of improving hydrometeorological forecasts have also been
1122 tested (Roux et al., 2020), pointing out the added value of ensemble strategies with
1123 respect to deterministic forecasts. Large meteorological ensemble spreads also allowed
1124 better threshold exceedance detection for flood warning. Furthermore, the rapid increase
1125 of total lightning flash rates has been found to be an important predictor for severe
1126 weather phenomena (e.g., Wu et al., 2018), which is closely related to the rapid increase
1127 of graupel concentration and updraft volumes in the mixed-phase layers of deep
1128 convective systems. Furthermore, many studies in the framework of the ST-lightning
1129 have been devoted to the examination of the relationship of lightning activity with
1130 microphysical properties of convective systems along their life cycle. During HyMeX
1131 SOP1, the HyMeX lightning mapping array network (HyLMA; Defer et al., 2015) was
1132 operated to locate and characterize the 3D lightning activity over the Cévenne-Vivarais

1133 area at flash, storm, and regional scales. This unique and comprehensive lightning data
1134 clearly showed the large potential for improving our knowledge about cloud
1135 microphysics, especially the distribution and evolution of ice hydrometeors by taking
1136 advantage of cloud electrification. This challenging subject is expected to be further
1137 addressed in near future.

1138

1139 The increased computational capacity, the development of high-resolution convection-
1140 permitting models and the availability of state-of-the-art observations have demonstrated
1141 to be of pivotal importance to attain a better understanding and modelling of HP in the
1142 last decade. Nevertheless, still the availability of observational data on the analysis of,
1143 e.g., small-scale processes, remains a limiting factor that challenges progress in process
1144 understanding and model evaluation, particularly when trying to underpin results from
1145 high-resolution model experiments with corresponding observations. Additionally,
1146 evaluation is expected to continue in those recent investigation lines developed within
1147 the HyMeX programme, which have already demonstrated their usefulness for
1148 advancing prediction or knowledge of HPE, such as CPEPS systems or the development
1149 and availability of fully coupled soil-vegetation-atmosphere-ocean models. Furthermore,
1150 the benefit of working under the umbrella of a long-lasting international experiment such
1151 as HyMeX allowed an effective and fruitful exchange of information on challenges,
1152 experiences, and goals, exploited through numerous multidisciplinary research activities.
1153 These interdisciplinary efforts were crucial to come towards improved understanding of
1154 the mechanisms leading to HP in the WMed. The links and networks originated in the
1155 framework of HyMeX must continue and even be enlarged in the future to progress
1156 together towards more integrated approaches. Novel integrated multidisciplinary
1157 research partnerships based on cross-sectional collaborations will be indeed needed to
1158 bridge more efficient research on impacts.

1159

1160 **Code and Data Availability**

1161 Given this is a review publication, the data and code availability are provided in each of
1162 the referenced publications.

1163

1164 **Author contributions**

1165 All authors collaborated and contributed to drafting, reviewing, and editing the paper. In
1166 particular, SK coordinated the effort and wrote the original draft; SD contributed to the
1167 reviewing of the low-level dynamical processes; PDG contributed to the reviewing of the
1168 observational capabilities; CLB contributed to the reviewing of the air-sea coupling; EF
1169 contributed to the reviewing of the large-scale dynamics; NF contributed to the reviewing
1170 of data assimilation; KOL contributed to the reviewing of the low-level dynamical
1171 processes; DR contributed to the reviewing of improved parameterizations; BV
1172 contributed to the reviewing of the microphysics; FB contributed to the reviewing of the
1173 predictability and ensemble forecast.

1174

1175 **Competing Interests**

1176 The authors declare that they have no conflict of interest.

1177

1178 **Acknowledgements**

1179 This work is a contribution to the HyMeX programme, supported in France by MISTRALS
1180 (Météo-France, CNRS, INRAE) and the Agence Nationale de la Recherche (ANR
1181 MUSIC grant ANR-14-CE01-0014, ANR IODA-MED grant ANR-11-BS56-0005). We
1182 would like to thank all HyMeX contributors, and particularly to all members of the
1183 scientific-team heavy precipitation (ST-HP), more than 100 in the last 10 years, which
1184 have effectively participated in advancing knowledge regarding heavy precipitation in the
1185 Mediterranean region. Without their work this study would not be possible. We further
1186 acknowledge the HyMeX database developers and all data providers.

1187 We also thank all HyMeX scientific team coordinators for the close cooperation during
1188 these years. We acknowledge H el ene Roux and Eric Defer for their input on research
1189 activities of the ST-ffv and ST-lightning. The authors thank Marie-No elle Bouin (CNRM
1190 & LOPS) who provided us MESO-NH simulation data related to IOP16a sensitivity to
1191 waves. The contribution of Paolo Di Girolamo to this work was possible based on the
1192 support from the Italian Ministry for Education, University and Research under the Grant
1193 OT4CLIMA and FISR2019_01711 CONCERNING. The contribution of the first author S.
1194 Khodayar Pardo was supported by the program Generacio Talent of Generalitat
1195 Valenciana (CIDEGENT/2018/017). Thank you to the two anonymous reviewers who
1196 helped us improved this manuscript with their comments.

1197

1198

1199 **References**

1200

1201 Adirosi, E., Gorgucci, E., Baldini, L. and Tokay, A.: Evaluation of Gamma Raindrop Size
1202 Distribution Assumption through Comparison of Rain Rates of Measured and Radar-
1203 Equivalent Gamma DSD, *Journal of Applied Meteorology and Climatology*, 53(6), 1618–
1204 1635, doi:10.1175/jamc-d-13-0150.1, 2014.

1205

1206 Adirosi, E., Baldini, L., Lombardo, F., Russo, F., Napolitano, F., Volpi, E. and Tokay, A.:
1207 Comparison of different fittings of drop spectra for rainfall retrievals, *Advances in Water*
1208 *Resources*, 83, 55–67, doi:10.1016/j.advwatres.2015.05.009, 2015.

1209

1210 Adirosi, E., Baldini, L., Roberto, N., Gatlin, P. and Tokay, A.: Improvement of vertical
1211 profiles of raindrop size distribution from micro rain radar using 2D video disdrometer
1212 measurements, *Atmospheric Research*, 169, 404–415,
1213 doi:10.1016/j.atmosres.2015.07.002, 2016.

1214

1215 Adler, B., Kalthoff, N., Kohler, M., Handwerker, J., Wieser, A., Corsmeier, U., Kottmeier,
1216 C., Lambert, D. and Bock, O.: The variability of water vapour and pre-convective
1217 conditions over the mountainous island of Corsica, *Quarterly Journal of the Royal*
1218 *Meteorological Society*, 142, 335–346, doi:10.1002/qj.2545, 2015.

1219

1220 Augros, C., Caumont, O., Ducrocq, V., Gaussiat, N. and Tabary, P.: Comparisons
1221 between S-, C- and X-band polarimetric radar observations and convective-scale
1222 simulations of the HyMeX first special observing period, *Quarterly Journal of the Royal*
1223 *Meteorological Society*, 142, 347–362, doi:10.1002/qj.2572, 2015.

1224

1225 Barthlott, C. and Kirshbaum, D. J.: Sensitivity of deep convection to terrain forcing over
1226 Mediterranean islands, *Quarterly Journal of the Royal Meteorological Society*, 139(676),
1227 1762–1779, doi:10.1002/qj.2089, 2013.

1228

1229 Barthlott, C., Adler, B., Kalthoff, N., Handwerker, J., Kohler, M. and Wieser, A.: The role
1230 of Corsica in initiating nocturnal offshore convection, *Quarterly Journal of the Royal*
1231 *Meteorological Society*, 142, 222–237, doi:10.1002/qj.2415, 2016.

1232

1233 Barthlott, C. and Davolio, S.: Mechanisms initiating heavy precipitation over Italy during
1234 HyMeX Special Observation Period 1: a numerical case study using two mesoscale

1235 models, *Quarterly Journal of the Royal Meteorological Society*, 142, 238–258,
1236 doi:10.1002/qj.2630, 2016.

1237

1238 Bassi, C.: Modelli meteorologici ad alta risoluzione: simulazione di episodi di
1239 precipitazione intensa in Liguria e Toscana durante la campagna HyMeX, Università di
1240 Milano, <https://www.sba.unimi.it/en/thesis/49.html>, 2014.

1241

1242 Bastin, S., Drobinski, P., Chiriaco, M., Bock, O., Roehrig, R., Gallardo, C., Conte, D.,
1243 Alonso, M. D., Li, L., Lionello, P. and Parracho, A. C.: Impact of humidity biases on light
1244 precipitation occurrence: observations versus simulations, *Atmospheric Chemistry and*
1245 *Physics*, 19(3), 1471–1490, doi:10.5194/acp-19-1471-2019, 2019.

1246

1247 Berthou, S., Mailler, S., Drobinski, P., Arsouze, T., Bastin, S., Béranger, K., Flaounas,
1248 E., Brossier, C. L., Somot, S. and Stéfanon, M.: Influence of submonthly air-sea coupling
1249 on heavy precipitation events in the Western Mediterranean basin, *Quarterly Journal of*
1250 *the Royal Meteorological Society*, 142, 453–471, doi:10.1002/qj.2717, 2016.

1251

1252 Berthou, S., Kendon, E. J., Chan, S. C., Ban, N., Leutwyler, D., Schär, C. and Fosser,
1253 G.: Pan-European climate at convection-permitting scale: a model intercomparison
1254 study, *Climate Dynamics*, 55(1-2), 35–59, doi:10.1007/s00382-018-4114-6, 2018.

1255

1256 Bock, O., Bosser, P., Pacione, R., Nuret, M., Fourrié, N. and Parracho, A.: A high-quality
1257 reprocessed ground-based GPS dataset for atmospheric process studies, radiosonde
1258 and model evaluation, and reanalysis of HyMeX Special Observing Period, *Quarterly*
1259 *Journal of the Royal Meteorological Society*, 142, 56–71, doi:10.1002/qj.2701, 2016.

1260

1261 Bonan, B., Albergel, C., Zheng, Y., Barbu, A. L., Fairbairn, D., Munier, S. and Calvet, J.-
1262 C.: An ensemble square root filter for the joint assimilation of surface soil moisture and
1263 leaf area index within the Land Data Assimilation System LDAS-Monde: application over
1264 the Euro-Mediterranean region, *Hydrology and Earth System Sciences*, 24(1), 325–347,
1265 doi:10.5194/hess-24-325-2020, 2020.

1266

1267 Borderies, M., Caumont, O., Delanoë, J., Ducrocq, V. and Fourrié, N.: Assimilation of
1268 wind data from airborne Doppler cloud-profiling radar in a kilometre-scale NWP system,
1269 *Natural Hazards and Earth System Sciences*, 19(4), 821–835, doi:10.5194/nhess-19-
1270 821-2019, 2019a.

1271

1272 Borderies, M., Caumont, O., Delanoë, J., Ducrocq, V., Fourrié, N. and Marquet, P.:
1273 Impact of airborne cloud radar reflectivity data assimilation on kilometre-scale numerical
1274 weather prediction analyses and forecasts of heavy precipitation events, *Natural*
1275 *Hazards and Earth System Sciences*, 19(4), 907–926, doi:10.5194/nhess-19-907-2019,
1276 2019b.
1277

1278 Borga, M., Comiti, F., Ruin, I. and Marra, F.: Forensic analysis of flash flood response,
1279 *WIREs Water*, 6(2), doi:10.1002/wat2.1338, 2019.
1280

1281 Bougeault, P., Binder, P., Buzzi, A., Dirks, R., Kuettner, J., Houze, R., Smith, R. B.,
1282 Steinacker, R. and Volkert, H.: The MAP Special Observing Period, *Bulletin of the*
1283 *American Meteorological Society*, 82(3), 433–462, doi:10.1175/1520-
1284 0477(2001)082<0433:tmsop>2.3.co;2, 2001.
1285

1286 Bouin, M.-N., Redelsperger, J.-L. and Brossier, C. L.: Processes leading to deep
1287 convection and sensitivity to sea-state representation during HyMeX IOP8 heavy
1288 precipitation event, *Quarterly Journal of the Royal Meteorological Society*,
1289 143(707), 2600–2615, doi:10.1002/qj.3111, 2017.
1290

1291 Bouttier, F., Raynaud, L., Nuissier, O. and Ménétrier, B.: Sensitivity of the AROME
1292 ensemble to initial and surface perturbations during HyMeX, *Quarterly Journal of the*
1293 *Royal Meteorological Society*, 142, 390–403, doi:10.1002/qj.2622, 2015.
1294

1295 Bresson, E., Ducrocq, V., Nuissier, O., Ricard, D. and de Saint-Aubin, C. (2012),
1296 Idealized numerical simulations of quasi-stationary convective systems over the
1297 Northwestern Mediterranean complex terrain. *Q.J.R. Meteorol. Soc.*, 138: 1751-1763.
1298 <https://doi.org/10.1002/qj.1911>
1299

1300 Brossier, C. L., Arsouze, T., Béranger, K., Bouin, M.-N., Bresson, E., Ducrocq, V.,
1301 Giordani, H., Nuret, M., Rainaud, R. and Taupier-Letage, I.: Ocean Mixed Layer
1302 responses to intense meteorological events during HyMeX-SOP1 from a high-resolution
1303 ocean simulation, *Ocean Modelling*, 84, 84–103, doi:10.1016/j.ocemod.2014.09.009,
1304 2014.
1305

1306 Buzzi, A., Davolio, S., Malguzzi, P., Drofa, O. and Mastrangelo, D.: Heavy rainfall
1307 episodes over Liguria in autumn 2011: numerical forecasting experiments, *Natural*

1308 Hazards and Earth System Sciences, 14(5), 1325–1340, doi:10.5194/nhess-14-1325-
1309 2014, 2014.
1310

1311 Caine, S., Lane, T. P., May, P. T., Jakob, C., Siems, S. T., Manton, M. J. and Pinto, J.:
1312 Statistical Assessment of Tropical Convection-Permitting Model Simulations Using a
1313 Cell-Tracking Algorithm, *Monthly Weather Review*, 141(2), 557–581, doi:10.1175/mwr-
1314 d-11-00274.1, 2013.
1315

1316 Caldas-Álvarez, A., Khodayar, S. and Bock, O.: GPS – Zenith Total Delay assimilation
1317 in different resolution simulations of a heavy precipitation event over southern France,
1318 *Advances in Science and Research*, 14, 157–162, doi:10.5194/asr-14-157-2017, 2017.
1319

1320 Caldas-Alvarez, A. and Khodayar, S.: Assessing atmospheric moisture effects on heavy
1321 precipitation during HyMeX IOP16 using GPS nudging and dynamical downscaling,
1322 *Natural Hazards and Earth System Sciences*, 20(10), 2753–2776, doi:10.5194/nhess-
1323 20-2753-2020, 2020.
1324

1325 Caldas-Alvarez, A., Khodayar, S., and Knippertz, P.: The impact of GPS and high-
1326 resolution radiosonde nudging on the simulation of heavy precipitation during HyMeX
1327 IOP6, *Weather Clim. Dynam.*, 2, 561–580, <https://doi.org/10.5194/wcd-2-561-2021>,
1328 2021.
1329

1330 Campins, J. and Navasqués, B. Impact of targeted observations on HIRLAM forecasts
1331 during HyMeX-SOP1. *Q.J.R. Meteorol. Soc.*, 142: 363-376.
1332 <https://doi.org/10.1002/qj.2737>, 2016.
1333

1334 Carrió, D.S., V. Homar, A. Jansà, M.A. Picornell, J. Campins, Diagnosis of a high-impact
1335 secondary cyclone during HyMeX-SOP1 IOP18, *Atmospheric Research*, Volume 242,
1336 2020, 104983, ISSN 0169-8095, <https://doi.org/10.1016/j.atmosres.2020.104983>.
1337

1338 Cavaleri, L., Bajo, M., Barbariol, F., Bastianini, M., Benetazzo, A., Bertotti, L., Chiggiato,
1339 J., Davolio, S., Ferrarin, C., Magnusson, L., Papa, A., Pezzutto, P., Pomaro, A. and
1340 Umgiesser, G.: The October 29, 2018 storm in Northern Italy – An exceptional event and
1341 its modeling, *Progress in Oceanography*, 178, 102178,
1342 doi:10.1016/j.pocean.2019.102178, 2019.
1343

1344 Chazette, P., Flamant, C., Raut, J.-C., Totems, J. and Shang, X.: Tropical moisture
1345 enriched storm tracks over the Mediterranean and their link with intense rainfall in the
1346 Cevennes-Vivarais area during HyMeX, *Quarterly Journal of the Royal Meteorological*
1347 *Society*, 142, 320–334, doi:10.1002/qj.2674, 2015a.

1348

1349 Chazette, P., Flamant, C., Shang, X., Totems, J., Raut, J.-C., Doerenbecher, A.,
1350 Ducrocq, V., Fourrié, N., Bock, O. and Cloché, S.: A multi-instrument and multi-model
1351 assessment of atmospheric moisture variability over the western Mediterranean during
1352 HyMeX, *Quarterly Journal of the Royal Meteorological Society*, 142, 7–22,
1353 doi:10.1002/qj.2671, 2015b.

1354

1355 Chazette, P., Totems, J., Ancellet, G., Pelon, J. and Sicard, M.: Temporal consistency of
1356 lidar observations during aerosol transport events in the framework of the
1357 ChArMEx/ADRIMED campaign at Minorca in June 2013, *Atmospheric Chemistry and*
1358 *Physics*, 16(5), 2863–2875, doi:10.5194/acp-16-2863-2016, 2016.

1359

1360 Clark, P., Roberts, N., Lean, H., Ballard, S. P. and Charlton-Perez, C.: Convection-
1361 permitting models: a step-change in rainfall forecasting, *Meteorological Applications*,
1362 23(2), 165–181, doi:10.1002/met.1538, 2016.

1363

1364 Colmet-Daage, A., Sanchez-Gomez, E., Ricci, S., Llovel, C., Estupina, V. B., Quintana-
1365 Seguí, P., Llasat, M. C. and Servat, E.: Evaluation of uncertainties in mean and extreme
1366 precipitation under climate changes for northwestern Mediterranean watersheds from
1367 high-resolution Med and Euro-CORDEX ensembles, doi:10.5194/hess-2017-49, 2017.

1368

1369 Coppola, E., Sobolowski, S., Pichelli, E., Raffaele, F., Ahrens, B., Anders, I., Ban, N.,
1370 Bastin, S., Belda, M., Belusic, D., Caldas-Alvarez, A., Cardoso, R. M., Davolio, S.,
1371 Dobler, A., Fernandez, J., Fita, L., Fumiere, Q., Giorgi, F., Goergen, K., Güttler, I.,
1372 Halenka, T., Heinzeller, D., Hodnebrog, Ø., Jacob, D., Kartsios, S., Katragkou, E.,
1373 Kendon, E., Khodayar, S., Kunstmann, H., Knist, S., Lavín-Gullón, A., Lind, P., Lorenz,
1374 T., Maraun, D., Marelle, L., van Meijgaard, E., Milovac, J., Myhre, G., Panitz, H.-J.,
1375 Piazza, M., Raffa, M., Raub, T., Rockel, B., Schär, C., Sieck, K., Soares, P. M. M., Somot,
1376 S., Srnec, L., Stocchi, P., Tölle, M. H., Truhetz, H., Vautard, R., de Vries, H. and Warrach-
1377 Sagi, K.: A first-of-its-kind multi-model convection permitting ensemble for investigating
1378 convective phenomena over Europe and the Mediterranean, *Climate Dynamics*, 55(1-2),
1379 3–34, doi:10.1007/s00382-018-4521-8, 2018.

1380

1381 Corsmeier, U., Hankers, R. and Wieser, A.: Airborne turbulence measurements in the
1382 lower troposphere onboard the research aircraft Dornier 128-6, D-IBUF,
1383 Meteorologische Zeitschrift, 10(4), 315–329, doi:10.1127/0941-2948/2001/0010-0315,
1384 2001.

1385

1386 Davolio, S., Mastrangelo, D., Miglietta, M. M., Drofa, O., Buzzi, A. and Malguzzi, P.: High
1387 resolution simulations of a flash flood near Venice, Natural Hazards and Earth System
1388 Sciences, 9(5), 1671–1678, doi:10.5194/nhess-9-1671-2009, 2009.

1389

1390 Davolio, S., Miglietta, M. M., Diomede, T., Marsigli, C. and Montani, A.: A flood episode
1391 in northern Italy: multi-model and single-model mesoscale meteorological ensembles for
1392 hydrological predictions, Hydrology and Earth System Sciences, 17(6), 2107–2120,
1393 doi:10.5194/hess-17-2107-2013, 2013.

1394

1395 Davolio, S., Silvestro, F. and Malguzzi, P.: Effects of Increasing Horizontal Resolution in
1396 a Convection-Permitting Model on Flood Forecasting: The 2011 Dramatic Events in
1397 Liguria, Italy, Journal of Hydrometeorology, 16(4), 1843–1856, doi:10.1175/jhm-d-14-
1398 0094.1, 2015.

1399

1400 Davolio, S., Henin, R., Stocchi, P. and Buzzi, A.: Bora wind and heavy persistent
1401 precipitation: atmospheric water balance and role of air-sea fluxes over the Adriatic Sea,
1402 Quarterly Journal of the Royal Meteorological Society, 143(703), 1165–1177,
1403 doi:10.1002/qj.3002, 2017.

1404

1405 Davolio, S., Della Fera, S., Laviola, S., Miglietta, M. M. and Levizzani, V.: Heavy
1406 Precipitation over Italy from the Mediterranean Storm” in October 2018: Assessing the
1407 Role of an Atmospheric River, Monthly Weather Review, 148(9), 3571–3588,
1408 doi:10.1175/mwr-d-20-0021.1, 2020.

1409

1410 Dayan, U., Nissen, K. and Ulbrich, U.: Review Article: Atmospheric conditions inducing
1411 extreme precipitation over the eastern and western Mediterranean, Natural Hazards and
1412 Earth System Sciences, 15(11), 2525–2544, doi:10.5194/nhess-15-2525-2015, 2015.

1413

1414 Defier, E., Pinty, J.-P., Coquillat, S., Martin, J.-M., Prieur, S., Soula, S., Richard, E., Rison,
1415 W., Krehbiel, P., Thomas, R., Rodeheffer, D., Vergeiner, C., Malaterre, F., Pedeboy, S.,
1416 Schulz, W., Farges, T., Gallin, L.-J., Ortéga, P., Ribaud, J.-F., Anderson, G., Betz, H.-D.,
1417 Meneux, B., Kotroni, V., Lagouvardos, K., Roos, S., Ducrocq, V., Roussot, O., Labatut,

1418 L. and Molinié, G.: An overview of the lightning and atmospheric electricity observations
1419 collected in southern France during the HYdrological cycle in Mediterranean EXperiment
1420 (HyMeX), Special Observation Period 1, Atmospheric Measurement Techniques, 8(2),
1421 649–669, doi:10.5194/amt-8-649-2015, 2015.

1422

1423 Diomede, T., Marsigli, C., Montani, A., Nerozzi, F. and Paccagnella, T.: Calibration of
1424 Limited-Area Ensemble Precipitation Forecasts for Hydrological Predictions, Monthly
1425 Weather Review, 142(6), 2176–2197, doi:10.1175/mwr-d-13-00071.1, 2014.

1426

1427 Doerenbecher, A., Basdevant, C., Drobinski, P., Durand, P., Fesquet, C., Bernard, F.,
1428 Cocquerez, P., Verdier, N. and Vargas, A.: Low-Atmosphere Drifting Balloons: Platforms
1429 for Environment Monitoring and Forecast Improvement, Bulletin of the American
1430 Meteorological Society, 97(9), 1583–1599, doi:10.1175/bams-d-14-00182.1, 2016.

1431

1432 Doocy, S., Daniels, A., Murray, S. and Kirsch, T. D.: The Human Impact of Floods: a
1433 Historical Review of Events 1980-2009 and Systematic Literature Review, PLoS
1434 Currents, doi:10.1371/currents.dis.f4deb457904936b07c09daa98ee8171a, 2013.

1435

1436 Draxler, R. R. and Hess, G. D.: An overview of the HYSPLIT_4 modelling system for
1437 trajectories, dispersion and deposition, Aust. Met. Mag., 47, 295–308, 1998.

1438

1439 Drobinski, P., Ducrocq, V., Alpert, P., Anagnostou, E., Béranger, K., Borga, M., Braud,
1440 I., Chanzy, A., Davolio, S., Delrieu, G., Estournel, C., Boubrahmi, N. F., Font, J., Grubišić,
1441 V., Gualdi, S., Homar, V., Ivančan-Picek, B., Kottmeier, C., Kotroni, V., Lagouvardos, K.,
1442 Lionello, P., Llasat, M. C., Ludwig, W., Lutoff, C., Mariotti, A., Richard, E., Romero, R.,
1443 Rotunno, R., Roussot, O., Ruin, I., Somot, S., Taupier-Letage, I., Tintore, J., Uijlenhoet,
1444 R. and Wernli, H.: HyMeX: A 10-Year Multidisciplinary Program on the Mediterranean
1445 Water Cycle, Bulletin of the American Meteorological Society, 95(7), 1063–1082,
1446 doi:10.1175/bams-d-12-00242.1, 2014.

1447

1448 Drobinski, P., Silva, N. D., Panthou, G., Bastin, S., Muller, C., Ahrens, B., Borga, M.,
1449 Conte, D., Fosser, G., Giorgi, F., Güttler, I., Kotroni, V., Li, L., Morin, E., Öno, B.,
1450 Quintana-Segui, P., Romera, R. and Torma, C. Z.: Scaling precipitation extremes with
1451 temperature in the Mediterranean: past climate assessment and projection in
1452 anthropogenic scenarios, Climate Dynamics, 51(3), 1237–1257, doi:10.1007/s00382-
1453 016-3083-x, 2016.

1454

1455 Ducrocq, V., Nuissier, O., Ricard, D., Lebeauvin, C. and Thouvenin, T.: A numerical
1456 study of three catastrophic precipitating events over southern France. II: Mesoscale
1457 triggering and stationarity factors, *Quarterly Journal of the Royal Meteorological Society*,
1458 134(630), 131–145, doi:10.1002/qj.199, 2008.

1459

1460 Ducrocq, V., Braud, I., Davolio, S., Ferretti, R., Flamant, C., Jansa, A., Kalthoff, N.,
1461 Richard, E., Taupier-Letage, I., Ayrat, P.-A., Belamari, S., Berne, A., Borga, M.,
1462 Boudevillain, B., Bock, O., Boichard, J.-L., Bouin, M.-N., Bousquet, O., Bouvier, C.,
1463 Chiggiato, J., Cimini, D., Corsmeier, U., Coppola, L., Cocquerez, P., Defer, E., Delanoë,
1464 J., Girolamo, P. D., Doerenbecher, A., Drobinski, P., Dufournet, Y., Fourrié, N., Gourley,
1465 J. J., Labatut, L., Lambert, D., Coz, J. L., Marzano, F. S., Molinié, G., Montani, A., Nord,
1466 G., Nuret, M., Ramage, K., Rison, W., Roussot, O., Said, F., Schwarzenboeck, A.,
1467 Testor, P., Baelen, J. V., Vincendon, B., Aran, M. and Tamayo, J.: HyMeX-SOP1: The
1468 Field Campaign Dedicated to Heavy Precipitation and Flash Flooding in the
1469 Northwestern Mediterranean, *Bulletin of the American Meteorological Society*, 95(7),
1470 1083–1100, doi:10.1175/bams-d-12-00244.1, 2014.

1471

1472 Duffourg, F. and Ducrocq, V.: Origin of the moisture feeding the Heavy Precipitating
1473 Systems over Southeastern France, *Natural Hazards and Earth System Sciences*, 11(4),
1474 1163–1178, doi:10.5194/nhess-11-1163-2011, 2011.

1475

1476 Duffourg, F. and Ducrocq, V.: Assessment of the water supply to Mediterranean heavy
1477 precipitation: a method based on finely designed water budgets, *Atmospheric Science*
1478 *Letters*, 14(3), 133–138, doi:10.1002/asl2.429, 2013.

1479

1480 Duffourg, F., Nuissier, O., Ducrocq, V., Flamant, C., Chazette, P., Delanoë, J.,
1481 Doerenbecher, A., Fourrié, N., Girolamo, P. D., Lac, C., Legain, D., Martinet, M., Saïd,
1482 F. and Bock, O.: Offshore deep convection initiation and maintenance during the HyMeX
1483 IOP 16a heavy precipitation event, *Quarterly Journal of the Royal Meteorological*
1484 *Society*, 142, 259–274, doi:10.1002/qj.2725, 2016.

1485

1486 Duffourg, F., Lee, K.-O., Ducrocq, V., Flamant, C., Chazette, P. and Girolamo, P. D.:
1487 Role of moisture patterns in the backbuilding formation of HyMeX IOP13 heavy
1488 precipitation systems, *Quarterly Journal of the Royal Meteorological Society*, 144(710),
1489 291–303, doi:10.1002/qj.3201, 2018.

1490

1491 Edouard, S., Vincendon, B. and Ducrocq, V.: Ensemble-based flash-flood modelling:
1492 Taking into account hydrodynamic parameters and initial soil moisture uncertainties,
1493 Journal of Hydrology, 560, 480–494, doi:10.1016/j.jhydrol.2017.04.048, 2018.

1494

1495 Federico, S., Torcasio, R. C., Avolio, E., Caumont, O., Montopoli, M., Baldini, L., Vulpiani,
1496 G. and Dietrich, S.: The impact of lightning and radar reflectivity factor data assimilation
1497 on the very short-term rainfall forecasts of RAMS@ISAC: application to two case studies
1498 in Italy, Natural Hazards and Earth System Sciences, 19(8), 1839–1864,
1499 doi:10.5194/nhess-19-1839-2019, 2019.

1500

1501 Fiori, E., Ferraris, L., Molini, L., Siccardi, F., Kranzmueller, D. and Parodi, A.: Triggering
1502 and evolution of a deep convective system in the Mediterranean Sea: modelling and
1503 observations at a very fine scale, Quarterly Journal of the Royal Meteorological Society,
1504 143(703), 927–941, doi:10.1002/qj.2977, 2017.

1505

1506 Flaounas, E., Raveh-Rubin, S., Wernli, H., Drobinski, P. and Bastin, S.: The dynamical
1507 structure of intense Mediterranean cyclones, Climate Dynamics, 44(9-10), 2411–2427,
1508 doi:10.1007/s00382-014-2330-2, 2014.

1509

1510 Flaounas, E., Lagouvardos, K., Kotroni, V., Claud, C., Delanoë, J., Flamant, C.,
1511 Madonna, E., and Wernli, H.: Processes leading to heavy precipitation associated with
1512 two Mediterranean cyclones observed during the HyMeX SOP1: Heavy Rainfall
1513 Associated with Two Cyclones during the HyMeX SOP1, Q.J.R. Meteorol. Soc., 142,
1514 275–286, <https://doi.org/10.1002/qj.2618>, 2016.

1515

1516 Flaounas, E., Luca, A. D., Drobinski, P., Mailler, S., Arsouze, T., Bastin, S., Beranger, K.
1517 and Brossier, C. L.: Cyclone contribution to the Mediterranean Sea water budget, Climate
1518 Dynamics, 46(3-4), 913–927, doi:10.1007/s00382-015-2622-1, 2015.

1519

1520 Flaounas, E., Kotroni, V., Lagouvardos, K., Gray, S. L., Rysman, J.-F., and Claud, C.:
1521 Heavy rainfall in Mediterranean cyclones. Part I: contribution of deep convection and
1522 warm conveyor belt, Clim Dyn, 50, 2935–2949, [https://doi.org/10.1007/s00382-017-](https://doi.org/10.1007/s00382-017-3783-x)
1523 [3783-x](https://doi.org/10.1007/s00382-017-3783-x), 2018.

1524

1525 Flaounas, E., Fita, L., Lagouvardos, K. and Kotroni, V.: Heavy rainfall in Mediterranean
1526 cyclones, Part II: Water budget, precipitation efficiency and remote water sources,
1527 Climate Dynamics, 53(5-6), 2539–2555, doi:10.1007/s00382-019-04639-x, 2019.

1528

1529 Fosser, G., Khodayar, S. and Berg, P.: Benefit of convection permitting climate model
1530 simulations in the representation of convective precipitation, *Climate Dynamics*, 44(1-2),
1531 45–60, doi:10.1007/s00382-014-2242-1, 2014.

1532

1533 Fourrié, N., Bresson, É., Nuret, M., Jany, C., Brousseau, P., Doerenbecher, A., Kreitz,
1534 M., Nuissier, O., Sevault, E., Bénichou, H., Amodei, M. and Pouponneau, F.: AROME-
1535 WMED, a real-time mesoscale model designed for the HyMeX special observation
1536 periods, *Geoscientific Model Development*, 8(7), 1919–1941, doi:10.5194/gmd-8-1919-
1537 2015, 2015.

1538

1539 Fourrié, N., Nuret, M., Brousseau, P., Caumont, O., Doerenbecher, A., Wattrelot, E.,
1540 Moll, P., Bénichou, H., Puech, D., Bock, O., Bosser, P., Chazette, P., Flamant, C.,
1541 Girolamo, P. D., Richard, E. and Saïd, F.: The AROME-WMED reanalyses of the first
1542 special observation period of the Hydrological cycle in the Mediterranean experiment
1543 (HyMeX), *Geoscientific Model Development*, 12(7), 2657–2678, doi:10.5194/gmd-12-
1544 2657-2019, 2019.

1545

1546 Fourrié, N., Nuret, M., Brousseau, P. and Caumont, O.: Data assimilation impact studies
1547 with the AROME-WMED reanalysis of the first special observation period of the
1548 Hydrological cycle in the Mediterranean Experiment, *Natural Hazards and Earth System*
1549 *Sciences*, 21(1), 463–480, doi:10.5194/nhess-21-463-2021, 2021.

1550

1551 Fresnay, S., Hally, A., Garnaud, C., Richard, E. and Lambert, D.: Heavy precipitation
1552 events in the Mediterranean: sensitivity to cloud physics parameterisation uncertainties,
1553 *Natural Hazards and Earth System Sciences*, 12(8), 2671–2688, doi:10.5194/nhess-12-
1554 2671-2012, 2012.

1555

1556 Fumière, Q., Déqué, M., Nuissier, O., Somot, S., Alias, A., Caillaud, C., Laurantin, O.
1557 and Seity, Y.: Extreme rainfall in Mediterranean France during the fall: added value of
1558 the CNRM-AROME Convection-Permitting Regional Climate Model, *Climate Dynamics*,
1559 55(1-2), 77–91, doi:10.1007/s00382-019-04898-8, 2019.

1560

1561 Funatsu, B. M., Claud, C. and Chaboureau, J.-P.: A 6-year AMSU-based climatology of
1562 upper-level troughs and associated precipitation distribution in the Mediterranean region,
1563 *Journal of Geophysical Research*, 113(D15), doi:10.1029/2008jd009918, 2008.

1564

1565 Galanaki, E., Flaounas, E., Kotroni, V., Lagouvardos, K. and Argiriou, A.: Lightning
1566 activity in the Mediterranean: quantification of cyclones contribution and relation to their
1567 intensity, *Atmospheric Science Letters*, 17(9), 510–516, doi:10.1002/asl.685, 2016.
1568

1569 Gao, X., Pal, J. S. and Giorgi, F.: Projected changes in mean and extreme precipitation
1570 over the Mediterranean region from a high resolution double nested RCM simulation,
1571 *Geophysical Research Letters*, 33(3), doi:10.1029/2005gl024954, 2006.
1572

1573 Giorgi, F.: Climate change hot-spots, *Geophysical Research Letters*, 33(8),
1574 doi:10.1029/2006gl025734, 2006.
1575

1576 Giorgi, F., Raffaele, F. and Coppola, E.: The response of precipitation characteristics to
1577 global warming from climate projections, *Earth System Dynamics*, 10(1), 73–89,
1578 doi:10.5194/esd-10-73-2019, 2019.
1579

1580 Giovannini, L., Davolio, S., Zaramella, M., Zardi, D. and Borga, M.: Multi-model
1581 convection-resolving simulations of the October 2018 Vaia storm over Northeastern Italy,
1582 *Atmospheric Research*, 253, 105455, doi:10.1016/j.atmosres.2021.105455, 2021.
1583

1584 Gires, A., Tchiguirinskaia, I., Schertzer, D. and Berne, A.: 2DVD Data Revisited:
1585 Multifractal Insights into Cuts of the Spatiotemporal Rainfall Process, *Journal of*
1586 *Hydrometeorology*, 16(2), 548–562, doi:10.1175/jhm-d-14-0127.1, 2015.
1587

1588 Di Girolamo, P., Summa, D., Lin, R.-F., Maestri, T., Rizzi, R. and Masiello, G.: UV Raman
1589 lidar measurements of relative humidity for the characterization of cirrus cloud
1590 microphysical properties, *Atmospheric Chemistry and Physics*, 9(22), 8799–8811,
1591 doi:10.5194/acp-9-8799-2009, 2009.
1592

1593 Di Girolamo, P., Flamant, C., Cacciani, M., Summa, D., Stelitano, D., Richard, E.,
1594 Ducrocq, V., Fourrie, N. and Said, F.: Lidar observations of low-level wind reversals over
1595 the Gulf of Lion and characterization of their impact on the water vapour variability,
1596 Author(s)., 2017.
1597

1598 Eckhardt, S., Stohl, A., Wernli, H., James, P., Forster, C., and Spichtinger, N.: A 15-Year
1599 Climatology of Warm Conveyor Belts, *J. Climate*, 17, 218–237, 2004

1600 Ferretti, R., Pichelli, E., Gentile, S., Maiello, I., Cimini, D., Davolio, S., Miglietta, M. M.,
1601 Panegrossi, G., Baldini, L., Pasi, F., Marzano, F. S., Zinzi, A., Mariani, S., Casaioli, M.,
1602 Bartolini, G., Loglisci, N., Montani, A., Marsigli, C., Manzato, A., Pucillo, A., Ferrario, M.
1603 E., Colaiuda, V., and Rotunno, R.: Overview of the first HyMeX Special Observation
1604 Period over Italy: observations and model results, *Hydrol. Earth Syst. Sci.*, 18, 1953–
1605 1977, <https://doi.org/10.5194/hess-18-1953-2014>, 2014.

1606

1607 Grams, C. M., Wernli, H., Böttcher, M., Čampa, J., Corsmeier, U., Jones, S. C., Keller,
1608 J. H., Lenz, C.-J. and Wiegand, L.: The key role of diabatic processes in modifying the
1609 upper-tropospheric wave guide: a North Atlantic case-study, *Quarterly Journal of the*
1610 *Royal Meteorological Society*, 137(661), 2174–2193, doi:10.1002/qj.891, 2011.

1611

1612 Grazioli, J., Tuia, D. and Berne, A.: Hydrometeor classification from polarimetric radar
1613 measurements: a clustering approach, *Atmospheric Measurement Techniques*, 8(1),
1614 149–170, doi:10.5194/amt-8-149-2015, 2015.

1615

1616 Grazzini, F., Craig, G. C., Keil, C., Antolini, G. and Pavan, V.: Extreme precipitation
1617 events over northern Italy. Part I: A systematic classification with machine-learning
1618 techniques, *Quarterly Journal of the Royal Meteorological Society*, 146(726), 69–85,
1619 doi:10.1002/qj.3635, 2019.

1620

1621 Grazzini, F., Fragkoulidis, G., Teubler, F., Wirth, V., Craig, GC. Extreme precipitation
1622 events over northern Italy. Part II: Dynamical precursors. *Q J R Meteorol Soc.* 2021; 147:
1623 1237– 1257. <https://doi.org/10.1002/qj.3969>

1624

1625 Hachani, S., Boudevillain, B., Delrieu, G. and Bargaoui, Z.: Drop Size Distribution
1626 Climatology in Cévennes-Vivarais Region, France, *Atmosphere*, 8(12), 233,
1627 doi:10.3390/atmos8120233, 2017.

1628

1629 Hally, A., Richard, E. and Ducrocq, V.: An ensemble study of HyMeX IOP6 and IOP7a:
1630 sensitivity to physical and initial and boundary condition uncertainties, *Natural Hazards*
1631 *and Earth System Sciences*, 14(5), 1071–1084, doi:10.5194/nhess-14-1071-2014, 2014.

1632

1633 Hally, A., Caumont, O., Garrote, L., Richard, E., Weerts, A., Delogu, F., Fiori, E., Rebora,
1634 N., Parodi, A., Mihalović, A., Ivković, M., Dekić, L., van Verseveld, W., Nuissier, O.,

1635 Ducrocq, V., Galizia, D. D. A., Danovaro, E. and Clematis, A.: Hydrometeorological multi-
1636 model ensemble simulations of the 4 November 2011 flash flood event in Genoa, Italy,
1637 in the framework of the DRIHM project, *Natural Hazards and Earth System Sciences*,
1638 15(3), 537–555, doi:10.5194/nhess-15-537-2015, 2015.

1639

1640 Hawcroft, M. K., Shaffrey, L. C., Hodges, K. I. and Dacre, H. F.: How much Northern
1641 Hemisphere precipitation is associated with extratropical cyclones?, *Geophysical*
1642 *Research Letters*, 39(24), doi:10.1029/2012gl053866, 2012.

1643

1644 Helgert, S. and Khodayar, S.: Improvement of the soil-atmosphere interactions and
1645 subsequent heavy precipitation modelling by enhanced initialization using remotely
1646 sensed 1 km soil moisture information, *Remote Sensing of Environment*, 246, 111812,
1647 doi:10.1016/j.rse.2020.111812, 2020.

1648

1649 Hertig, E., Trambly, Y., Romberg, K., Kaspar-Ott, I. and Merckenschlager, C.: The impact
1650 of soil moisture on precipitation downscaling in the Euro-Mediterranean area, *Climate*
1651 *Dynamics*, 52(5-6), 2869–2884, doi:10.1007/s00382-018-4304-2, 2018.

1652

1653 Homar, V., Ramis, C., Romero, R., Alonso, S., Garcia-Moya, J. A. and Alarcon, M.: A
1654 Case of Convection Development over the Western Mediterranean Sea: A Study through
1655 Numerical Simulations, *Meteorology and Atmospheric Physics*, 71(3-4), 169–188,
1656 doi:10.1007/s007030050054, 1999.

1657

1658 Insua-Costa, D., Miguez-Macho, G., and Llasat, M. C.: Local and remote moisture
1659 sources for extreme precipitation: a study of the two catastrophic 1982 western
1660 Mediterranean episodes, *Hydrol. Earth Syst. Sci.*, 23, 3885–3900,
1661 <https://doi.org/10.5194/hess-23-3885-2019>, 2019.

1662

1663 IPCC: *Climate Change 2013: The Physical Science Basis. Contribution of Working*
1664 *Group I to the Fifth Assessment Report of the Intergovernmental Panel on Climate*
1665 *Change* [Stocker, T.F., D. Qin, G.-K. Plattner, M. Tignor, S.K. Allen, J. Boschung, A.
1666 Nauels, Y. Xia, V. Bex and P.M. Midgley (eds.)], edited by I. P. on Climate Change,
1667 Cambridge University Press., 2009.

1668

1669 Jacob, D., Petersen, J., Eggert, B., Alias, A., Christensen, O. B., Bouwer, L. M., Braun,
1670 A., Colette, A., Déqué, M., Georgievski, G., Georgopoulou, E., Gobiet, A., Menut, L.,
1671 Nikulin, G., Haensler, A., Hempelmann, N., Jones, C., Keuler, K., Kovats, S., Kröner, N.,

1672 Kotlarski, S., Kriegsmann, A., Martin, E., van Meijgaard, E., Moseley, C., Pfeifer, S.,
1673 Preuschmann, S., Radermacher, C., Radtke, K., Rechid, D., Rounsevell, M.,
1674 Samuelsson, P., Somot, S., Soussana, J.-F., Teichmann, C., Valentini, R., Vautard, R.,
1675 Weber, B. and Yiou, P.: EURO-CORDEX: new high-resolution climate change
1676 projections for European impact research, *Regional Environmental Change*, 14(2), 563–
1677 578, doi:10.1007/s10113-013-0499-2, 2013.

1678

1679 Jansa, A., Genoves, A., Picornell, M. A., Campins, J., Riosalido, R. and Carretero, O.:
1680 Western Mediterranean cyclones and heavy rain. Part 2: Statistical approach,
1681 *Meteorological Applications*, 8(1), 43–56, doi:10.1017/s1350482701001049, 2001.

1682

1683 Jansa, A., Campins, J., Picornell, M.A, Guijarro, J.. Heavy rain and strong wind events
1684 over Spain during HyMeX SOP1. *Tethys*. 11. 25 - 38. 10.3369/tethys.2014.11.03, 2014.

1685

1686 Jianyun, G., Ziwang, D. and Xiaolan, Z.: Spatial/temporal features of drought/flood in
1687 Fujian for the past 4 decades, *Journal of Tropical Meteorology*, 22(5), 491–497, 2006.

1688

1689 Kagkara, C., Wobrock, W., Planche, C. and Flossmann, A. I.: The sensitivity of intense
1690 rainfall to aerosol particle loading – a comparison of bin-resolved microphysics modelling
1691 with observations of heavy precipitation from HyMeX IOP7a, *Natural Hazards and Earth
1692 System Sciences*, 20(5), 1469–1483, doi:10.5194/nhess-20-1469-2020, 2020.

1693

1694 Kalthoff, N., Adler, B., Wieser, A., Kohler, M., Träumner, K., Handwerker, J., Corsmeier,
1695 U., Khodayar, S., Lambert, D., Kopmann, A., Kunka, N., Dick, G., Ramatschi, M.,
1696 Wickert, J. and Kottmeier, C.: KITcube a mobile observation platform for convection
1697 studies deployed during HyMeX, *Meteorologische Zeitschrift*, 22(6), 633–647,
1698 doi:10.1127/0941-2948/2013/0542, 2013.

1699

1700 Khodayar, S., Czajka, B., Caldas-Alvarez, A., Helgert, S., Flamant, C., Girolamo, P. D.,
1701 Bock, O. and Chazette, P.: Multi-scale observations of atmospheric moisture variability
1702 in relation to heavy precipitating systems in the northwestern Mediterranean during
1703 HyMeX IOP12, *Quarterly Journal of the Royal Meteorological Society*, 144(717), 2761–
1704 2780, doi:10.1002/qj.3402, 2018.

1705

1706 Khodayar, S., Fosser, G., Berthou, S., Davolio, S., Drobinski, P., Ducrocq, V., Ferretti,
1707 R., Nuret, M., Pichelli, E., Richard, E. and Bock, O.: A seamless weather-climate multi-
1708 model intercomparison on the representation of a high impact weather event in the

1709 western Mediterranean: HyMeX IOP12, Quarterly Journal of the Royal Meteorological
1710 Society, 142, 433–452, doi:10.1002/qj.2700, 2016a.
1711

1712 Khodayar, S., Kalthoff, N. and Kottmeier, C.: Atmospheric conditions associated with
1713 heavy precipitation events in comparison to seasonal means in the western
1714 mediterranean region, *Climate Dynamics*, 51(3), 951–967, doi:10.1007/s00382-016-
1715 3058-y, 2016b.
1716

1717 Khodayar, S., Raff, F., Kalthoff, N. and Bock, O.: Diagnostic study of a high-precipitation
1718 event in the Western Mediterranean: adequacy of current operational networks,
1719 Quarterly Journal of the Royal Meteorological Society, 142, 72–85, doi:10.1002/qj.2600,
1720 2015.
1721

1722 Kirshbaum, D. J., Adler, B., Kalthoff, N., Barthlott, C. and Serafin S.: Moist orographic
1723 convection: Physical mechanisms and links to surface-exchange processes,
1724 *Atmosphere*, 9(3):80. <https://doi.org/10.3390/atmos9030080>, 2018.
1725

1726 Krichak, S. O., Feldstein, S. B., Alpert, P., Gualdi, S., Scoccimarro, E. and Yano, J.-I.:
1727 Discussing the role of tropical and subtropical moisture sources in extreme precipitation
1728 events in the Mediterranean region from a climate change perspective,
1729 doi:10.5194/nhessd-3-3983-2015, 2015.
1730

1731 Lebeaupin-, C., Ducrocq, V. and Giordani, H.: Sensitivity of torrential rain events to the
1732 sea surface temperature based on high-resolution numerical forecasts, *Journal of*
1733 *Geophysical Research*, 111(D12), doi:10.1029/2005jd006541, 2006.
1734

1735 Lebeaupin-Brossier, C., Bastin, S., Béranger, K. and Drobinski, P.: Regional mesoscale
1736 air–sea coupling impacts and extreme meteorological events role on the Mediterranean
1737 Sea water budget, *Climate Dynamics*, 44(3-4), 1029–1051, doi:10.1007/s00382-014-
1738 2252-z, 2014.

1739 Lee, K.-O., Flamant, C., Ducrocq, V., Duffourg, F., Fourrié, N. and Davolio, S.:
1740 Convective initiation and maintenance processes of two back-building mesoscale
1741 convective systems leading to heavy precipitation events in Southern Italy during HyMeX
1742 IOP 13, Quarterly Journal of the Royal Meteorological Society, 142(700), 2623–2635,
1743 doi:10.1002/qj.2851, 2016.
1744

1745 Lee, K.-O., Flamant, C., Ducrocq, V., Duffourg, F., Fourrié, N., Delanoë, J. and Bech, J.:
1746 Initiation and development of a mesoscale convective system in the Ebro River Valley
1747 and related heavy precipitation over northeastern Spain during HyMeX IOP 15a,
1748 Quarterly Journal of the Royal Meteorological Society, 143(703), 942–956,
1749 doi:10.1002/qj.2978, 2017.

1750

1751 Lee, K.-O., Flamant, C., Duffourg, F., Ducrocq, V. and Chaboureau, J.-P.: Impact of
1752 upstream moisture structure on a back-building convective precipitation system in south-
1753 eastern France during HyMeX IOP13, Atmospheric Chemistry and Physics, 18(23),
1754 16845–16862, doi:10.5194/acp-18-16845-2018, 2018.

1755

1756 Lee, K.-O., Aemisegger, F., Pfahl, S., Flamant, C., Lacour, J.-L. and Chaboureau, J.-P.:
1757 Contrasting stable water isotope signals from convective and large-scale precipitation
1758 phases of a heavy precipitation event in southern Italy during HyMeX IOP 13: a modelling
1759 perspective, Atmospheric Chemistry and Physics, 19(11), 7487–7506, doi:10.5194/acp-
1760 19-7487-2019, 2019.

1761

1762 Lindskog, M., Ridal, M., Thorsteinsson, S. and Ning, T.: Data assimilation of GNSS
1763 zenith total delays from a Nordic processing centre, Atmospheric Chemistry and Physics,
1764 17(22), 13983–13998, doi:10.5194/acp-17-13983-2017, 2017.

1765

1766 Llasat, M. C., Llasat-Botija, M., Prat, M. A., Porcú, F., Price, C., Mugnai, A., Lagouvardos,
1767 K., Kotroni, V., Katsanos, D., Michaelides, S., Yair, Y., Savvidou, K. and
1768 Nicolaidis, K.: High-impact floods and flash floods in Mediterranean countries: the
1769 FLASH preliminary database, Advances in Geosciences, 23, 47–55, doi:10.5194/adgeo-
1770 23-47-2010, 2010.

1771

1772 Lovat, A., Vincendon, B. and Ducrocq, V.: Assessing the impact of resolution and soil
1773 datasets on flash-flood modelling, Hydrology and Earth System Sciences, 23(3), 1801–
1774 1818, doi:10.5194/hess-23-1801-2019, 2019.

1775

1776 Madonna, E., Wernli, H., Joos, H., and Martius, O.: Warm conveyor belts in the ERA-
1777 Interim dataset (1979–2010). Part I: Climatology and potential vorticity evolution, J.
1778 Climate, 27, 3–26, doi:10.1175/jcli-d-12-00720.1, 2014.

1779

1780 Magnusson, L., Hewson, T. and Lavers, D.: Windstorm Alex affected large parts of
1781 Europe, *ECMWF Newsletter*, 166, 4–5, 2021.
1782

1783 Maiello, I., Gentile, S., Ferretti, R., Baldini, L., Roberto, N., Picciotti, E., Alberoni, P. P.
1784 and Marzano, F. S.: Impact of multiple radar reflectivity data assimilation on the
1785 numerical simulation of a flash flood event during the HyMeX campaign, *Hydrology and*
1786 *Earth System Sciences*, 21(11), 5459–5476, doi:10.5194/hess-21-5459-2017, 2017.
1787

1788 Manzato, A., Davolio, S., Miglietta, M. M., Pucillo, A. and Setvák, M.: 12 September
1789 2012: A supercell outbreak in NE Italy?, *Atmospheric Research*, 153, 98–118,
1790 doi:10.1016/j.atmosres.2014.07.019, 2015.
1791

1792 Mariotti, A.: Recent Changes in the Mediterranean Water Cycle: A Pathway toward Long-
1793 Term Regional Hydroclimatic Change?, *Journal of Climate*, 23(6), 1513–1525,
1794 doi:10.1175/2009jcli3251.1, 2010.
1795

1796 Marsigli, C., Montani, A. and Paccagnella, T.: Provision of boundary conditions for a
1797 convection-permitting ensemble: comparison of two different approaches, *Nonlinear*
1798 *Processes in Geophysics*, 21(2), 393–403, doi:10.5194/npg-21-393-2014, 2014.
1799

1800 Martinet, M., Nuissier, O., Duffourg, F., Ducrocq, V. and Ricard, D.: Fine-scale numerical
1801 analysis of the sensitivity of the HyMeX IOP16a heavy precipitating event to the turbulent
1802 mixing-length parametrization, *Quarterly Journal of the Royal Meteorological Society*,
1803 143(709), 3122–3135, doi:10.1002/qj.3167, 2017.
1804

1805 Mastrantonas, N, Herrera-Lormendez, P, Magnusson, L, Pappenberger, F, Matschullat,
1806 J. Extreme precipitation events in the Mediterranean: Spatiotemporal characteristics and
1807 connection to large-scale atmospheric flow patterns. *Int J Climatol*. 2021; 41: 2710–
1808 2728. <https://doi.org/10.1002/joc.6985>
1809

1810 Meroni, A. N., Parodi, A. and Pasquero, C.: Role of SST Patterns on Surface Wind
1811 Modulation of a Heavy Midlatitude Precipitation Event, *Journal of Geophysical Research:*
1812 *Atmospheres*, 123(17), 9081–9096, doi:10.1029/2018jd028276, 2018a.
1813

1814 Meroni, A. N., Renault, L., Parodi, A. and Pasquero, C.: Role of the Oceanic Vertical
1815 Thermal Structure in the Modulation of Heavy Precipitations Over the Ligurian Sea, *Pure*
1816 *and Applied Geophysics*, 175(11), 4111–4130, doi:10.1007/s00024-018-2002-y, 2018b.

1817
1818 Miglietta, M. M. and Rotunno, R.: Numerical Simulations of Conditionally Unstable Flows
1819 over a Mountain Ridge, *Journal of the Atmospheric Sciences*, 66(7), 1865–1885,
1820 doi:10.1175/2009jas2902.1, 2009.
1821
1822 Miglietta, M. M. and Rotunno, R.: Numerical Simulations of Sheared Conditionally
1823 Unstable Flows over a Mountain Ridge, *Journal of the Atmospheric Sciences*, 71(5),
1824 1747–1762, doi:10.1175/jas-d-13-0297.1, 2014.
1825
1826 Miglietta, M. M., Manzato, A. and Rotunno, R.: Characteristics and predictability of a
1827 supercell during HyMeX SOP1, *Quarterly Journal of the Royal Meteorological Society*,
1828 142(700), 2839–2853, doi:10.1002/qj.2872, 2016.
1829
1830 Moeng, C.-H., Sullivan, P. P., Khairoutdinov, M. F. and Randall, D. A.: A Mixed Scheme
1831 for Subgrid-Scale Fluxes in Cloud-Resolving Models, *Journal of the Atmospheric*
1832 *Sciences*, 67(11), 3692–3705, doi:10.1175/2010jas3565.1, 2010.
1833
1834 Molinié, G., Ceresetti, D., Anquetin, S., Creutin, J. D. and Boudevillain, B.: Rainfall
1835 Regime of a Mountainous Mediterranean Region: Statistical Analysis at Short Time
1836 Steps, *Journal of Applied Meteorology and Climatology*, 51(3), 429–448,
1837 doi:10.1175/2011jamc2691.1, 2012.
1838
1839 Nelson, G. C., Rosegrant, M. W., Palazzo, A., Gray, I., Ingersoll, C., Robertson, R.,
1840 Tokgoz, S., Zhu, T., Sulser, T. B., Ringler, C., Msangi, S. and You, L.: Food Security,
1841 Farming, and Climate Change to 2050: Scenarios, Results, Policy Options, International
1842 Food Policy Research Institute., 2010.
1843
1844 Nielsen, E. R. and Schumacher, R. S.: Using Convection-Allowing Ensembles to
1845 Understand the Predictability of an Extreme Rainfall Event, *Monthly Weather Review*,
1846 144(10), 3651–3676, doi:10.1175/mwr-d-16-0083.1, 2016.
1847
1848 Nuissier, O., Ducrocq, V., Ricard, D., Lebeaupin, C. and Anquetin, S.: A numerical study
1849 of three catastrophic precipitating events over southern France. I: Numerical framework
1850 and synoptic ingredients, *Quarterly Journal of the Royal Meteorological Society*,
1851 134(630), 111–130, doi:10.1002/qj.200, 2008.
1852

1853 Nuissier, O., Joly, B., Joly, A., Ducrocq, V. and Arbogast, P.: A statistical downscaling to
1854 identify the large-scale circulation patterns associated with heavy precipitation events
1855 over southern France, *Quarterly Journal of the Royal Meteorological Society*, 137(660),
1856 1812–1827, doi:10.1002/qj.866, 2011.

1857

1858 Nuissier, O., Joly, B., Vié, B. and Ducrocq, V.: Uncertainty of lateral boundary conditions
1859 in a convection-permitting ensemble: a strategy of selection for Mediterranean heavy
1860 precipitation events, *Natural Hazards and Earth System Sciences*, 12(10), 2993–3011,
1861 doi:10.5194/nhess-12-2993-2012, 2012.

1862

1863 Nuissier, O., Marsigli, C., Vincendon, B., Hally, A., Bouttier, F., Montani, A. and
1864 Paccagnella, T.: Evaluation of two convection-permitting ensemble systems in the
1865 HyMeX Special Observation Period (SOP1) framework, *Quarterly Journal of the Royal*
1866 *Meteorological Society*, 142, 404–418, doi:10.1002/qj.2859, 2016.

1867

1868 Nuissier, O., Duffourg, F., Martinet, M., Ducrocq, V. and Lac, C.: Hectometric-scale
1869 simulations of a Mediterranean heavy-precipitation event during the Hydrological cycle
1870 in the Mediterranean Experiment (HyMeX) first Special Observation Period (SOP1),
1871 *Atmospheric Chemistry and Physics*, 20(23), 14649–14667, doi:10.5194/acp-20-14649-
1872 2020, 2020.

1873

1874 Oertel, A., Boettcher, M., Joos, H., Sprenger, M., Konow, H., Hagen, M. and Wernli, H.:
1875 Convective activity in an extratropical cyclone and its warm conveyor belt – a case-study
1876 combining observations and a convection-permitting model simulation, *Quarterly Journal*
1877 *of the Royal Meteorological Society*, 145(721), 1406–1426, doi:10.1002/qj.3500, 2019.

1878 Oost, W. A., Komen, G. J., Jacobs, C. M. J. and Oort, C. V.: New evidence for a relation
1879 between wind stress and wave age from measurements during ASGAMAGE, *Boundary-*
1880 *Layer Meteorology*, 103(3), 409–438, doi:10.1023/a:1014913624535, 2002.

1881 Orłowsky, B. and Seneviratne, S. I.: Global changes in extreme events: regional and
1882 seasonal dimension, *Climatic Change*, 110(3-4), 669–696, doi:10.1007/s10584-011-
1883 0122-9, 2011.

1884

1885 Papagiannaki, K., Kotroni, V., Lagouvardos, K., Ruin, I. and Bezes, A.: Urban Area
1886 Response to Flash Flood–Triggering Rainfall, Featuring Human Behavioral Factors: The
1887 Case of 22 October 2015 in Attica, Greece, *Weather, Climate, and Society*, 9(3), 621–
1888 638, doi:10.1175/wcas-d-16-0068.1, 2017.

1889

1890 Pfahl, S., Madonna, E., Boettcher, M., Joos, H. and Wernli, H.: Warm Conveyor Belts in
1891 the ERA-Interim Dataset (1979–2010). Part II: Moisture Origin and Relevance for
1892 Precipitation, *Journal of Climate*, 27(1), 27–40, doi:10.1175/jcli-d-13-00223.1, 2014.

1893 Pichelli, E., Rotunno, R. and Ferretti, R.: Effects of the Alps and Apennines on forecasts
1894 for Po Valley convection in two HyMeX cases, *Quarterly Journal of the Royal
1895 Meteorological Society*, 143(707), 2420–2435, doi:10.1002/qj.3096, 2017.

1896

1897 Planton, S., Driouech, F., Rhaz, K. E. and Lionello, P.: The climate of the Mediterranean
1898 regions in the future climate projections. In: *The Mediterranean region under climate
1899 change*, p.86., 2016.

1900

1901 Poletti, M. L., Silvestro, F., Davolio, S., Pignone, F. and Rebora, N.: Using nowcasting
1902 technique and data assimilation in a meteorological model to improve very short range
1903 hydrological forecasts, *Hydrology and Earth System Sciences*, 23(9), 3823–3841,
1904 doi:10.5194/hess-23-3823-2019, 2019.

1905

1906 Prein, A. F., Langhans, W., Fosser, G., Ferrone, A., Ban, N., Goergen, K., Keller, M.,
1907 Tölle, M., Gutjahr, O., Feser, F., Brisson, E., Kollet, S., Schmidli, J., Lipzig, N. P. M. and
1908 Leung, R.: A review on regional convection-permitting climate modeling:
1909 Demonstrations, prospects, and challenges, *Reviews of Geophysics*, 53(2), 323–361,
1910 doi:10.1002/2014rg000475, 2015.

1911

1912 Protat, A., Bouniol, D., Delanoë, J., O'Connor, E., May, P. T., Plana-Fattori, A., Hasson,
1913 A., Görsdorf, U. and Heymsfield, A. J.: Assessment of Cloudsat Reflectivity
1914 Measurements and Ice Cloud Properties Using Ground-Based and Airborne Cloud
1915 Radar Observations, *Journal of Atmospheric and Oceanic Technology*, 26(9), 1717–
1916 1741, doi:10.1175/2009jtecha1246.1, 2009.

1917

1918 Rainaud, R., Brossier, C. L., Ducrocq, V., Giordani, H., Nuret, M., Fourrié, N., Bouin, M.-
1919 N., Taupier-Letage, I. and Legain, D.: Characterization of air-sea exchanges over the
1920 Western Mediterranean Sea during HyMeX SOP1 using the AROME-WMED model,
1921 *Quarterly Journal of the Royal Meteorological Society*, 142, 173–187,
1922 doi:10.1002/qj.2480, 2015.

1923

1924 Rainaud, R., Brossier, C. L., Ducrocq, V. and Giordani, H.: High-resolution air-sea
1925 coupling impact on two heavy precipitation events in the Western Mediterranean,

1926 Quarterly Journal of the Royal Meteorological Society, 143(707), 2448–2462,
1927 doi:10.1002/qj.3098, 2017.
1928
1929 Ramis, C., Llasat, M.C., Genovés, A. and Jansà, A. (1994), The October-1987 floods in
1930 Catalonia: Synoptic and mesoscale mechanisms. Met. Apps, 1: 337-
1931 350. <https://doi.org/10.1002/met.5060010404>
1932
1933 Raupach, T. H. and Berne, A.: Small-Scale Variability of the Raindrop Size Distribution
1934 and Its Effect on Areal Rainfall Retrieval, Journal of Hydrometeorology, 17(7), 2077–
1935 2104, doi:10.1175/jhm-d-15-0214.1, 2016.
1936
1937 Ravazzani, G., Amengual, A., Ceppi, A., Homar, V., Romero, R., Lombardi, G. and
1938 Mancini, M.: Potentialities of ensemble strategies for flood forecasting over the Milano
1939 urban area, Journal of Hydrology, 539, 237–253, doi:10.1016/j.jhydrol.2016.05.023,
1940 2016.
1941
1942 Raveh-Rubin, S. and Flaounas, E.: A dynamical link between deep Atlantic extratropical
1943 cyclones and intense Mediterranean cyclones, Atmospheric Science Letters, 18(5), 215–
1944 221, doi:10.1002/asl.745, 2017.
1945
1946 Raveh-Rubin, S. and Wernli, H.: Large-scale wind and precipitation extremes in the
1947 Mediterranean: a climatological analysis for 1979-2012, Quarterly Journal of the Royal
1948 Meteorological Society, 141(691), 2404–2417, doi:10.1002/qj.2531, 2015.
1949
1950 Raynaud, L. and Bouttier, F.: Comparison of initial perturbation methods for ensemble
1951 prediction at convective scale, Quarterly Journal of the Royal Meteorological Society,
1952 142(695), 854–866, doi:10.1002/qj.2686, 2015.
1953
1954 Rebora, N., Molini, L., Casella, E., Comellas, A., Fiori, E., Pignone, F., Siccardi, F.,
1955 Silvestro, F., Tanelli, S. and Parodi, A.: Extreme Rainfall in the Mediterranean: What Can
1956 We Learn from Observations?, Journal of Hydrometeorology, 14(3), 906–922,
1957 doi:10.1175/jhm-d-12-083.1, 2013.
1958
1959 Ribaud, J.-F., Bousquet, O., Coquillat, S., Al-Sakka, H., Lambert, D., Ducrocq, V. and
1960 Fontaine, E.: Evaluation and application of hydrometeor classification algorithm outputs
1961 inferred from multi-frequency dual-polarimetric radar observations collected during

1962 HyMeX, *Quarterly Journal of the Royal Meteorological Society*, 142, 95–107,
1963 doi:10.1002/qj.2589, 2015.

1964

1965 Ribaud, J.-F., Bousquet, O. and Coquillat, S.: Relationships between total lightning
1966 activity, microphysics and kinematics during the 24 September 2012 HyMeX bow-echo
1967 system, *Quarterly Journal of the Royal Meteorological Society*, 142, 298–309,
1968 doi:10.1002/qj.2756, 2016.

1969

1970 Ricard, D., Ducrocq, V. and Auger, L.: A Climatology of the Mesoscale Environment
1971 Associated with Heavily Precipitating Events over a Northwestern Mediterranean Area,
1972 *Journal of Applied Meteorology and Climatology*, 51(3), 468–488, doi:10.1175/jamc-d-
1973 11-017.1, 2012.

1974

1975 Richard, E., Buzzi, A. and Zängl, G.: Quantitative precipitation forecasting in the Alps:
1976 The advances achieved by the Mesoscale Alpine Programme, *Quarterly Journal of the*
1977 *Royal Meteorological Society*, 133(625), 831–846, doi:10.1002/qj.65, 2007.

1978

1979 Röhner, L., Nerding, K.-U. and Corsmeier, U.: Diagnostic study of a HyMeX heavy
1980 precipitation event over Spain by investigation of moisture trajectories, *Quarterly Journal*
1981 *of the Royal Meteorological Society*, 142, 287–297, doi:10.1002/qj.2825, 2016.

1982 Rolph, G., Stein, A. and Stunder, B.: Real-time Environmental Applications and Display
1983 sYstem: READY, *Environmental Modelling & Software*, 95, 210–228,
1984 doi:10.1016/j.envsoft.2017.06.025, 2017.

1985

1986 Romero, R., Ramis, C. and Homar, V.: On the severe convective storm of 29 October
1987 2013 in the Balearic Islands: observational and numerical study, *Quarterly Journal of the*
1988 *Royal Meteorological Society*, 141(689), 1208–1222, doi:10.1002/qj.2429, 2014.

1989 Roux, H., Amengual, A., Romero, R., Bladé, E. and Sanz-Ramos, M.: Evaluation of two
1990 hydrometeorological ensemble strategies for flash-flood forecasting over a catchment of
1991 the eastern Pyrenees, *Natural Hazards and Earth System Sciences*, 20(2), 425–450,
1992 doi:10.5194/nhess-20-425-2020, 2020.

1993

1994 Ruin, I., Lutoff, C., Boudevillain, B., Creutin, J.-D., Anquetin, S., Rojo, M. B., Boissier, L.,
1995 Bonnifait, L., Borga, M., Colbeau-Justin, L., Creton-Cazanave, L., Delrieu, G., Douvinet,
1996 J., Gaume, E., Grunfest, E., Naulin, J.-P., Payrastre, O. and Vannier, O.: Social and
1997 Hydrological Responses to Extreme Precipitations: An Interdisciplinary Strategy for

1998 Postflood Investigation, *Weather, Climate, and Society*, 6(1), 135–153,
1999 doi:10.1175/wcas-d-13-00009.1, 2014.
2000
2001 Sauvage, C., Brossier, C. L., Bouin, M.-N. and Ducrocq, V.: Characterization of the air–
2002 sea exchange mechanisms during a Mediterranean heavy precipitation event using
2003 realistic sea state modelling, *Atmospheric Chemistry and Physics*, 20(3), 1675–1699,
2004 doi:10.5194/acp-20-1675-2020, 2020.
2005
2006 Scheffknecht, P., Richard, E. and Lambert, D.: A highly localized high-precipitation event
2007 over Corsica, *Quarterly Journal of the Royal Meteorological Society*, 142, 206–221,
2008 doi:10.1002/qj.2795, 2016.
2009
2010 Scheffknecht, P., Richard, E. and Lambert, D.: Climatology of heavy precipitation over
2011 Corsica in the period 1985-2015, *Quarterly Journal of the Royal Meteorological Society*,
2012 143(709), 2987–2998, doi:10.1002/qj.3140, 2017.
2013
2014 Schleiss, M. and Smith, J.: A Method to Estimate the 3D–Time Structure of the Raindrop
2015 Size Distribution Using Radar and Disdrometer Data*, *Journal of Hydrometeorology*,
2016 16(3), 1222–1242, doi:10.1175/jhm-d-14-0182.1, 2015.
2017
2018 Schumacher, R. S. and Johnson, R. H.: Organization and Environmental Properties of
2019 Extreme-Rain-Producing Mesoscale Convective Systems, *Monthly Weather Review*,
2020 133(4), 961–976, doi:10.1175/mwr2899.1, 2005.
2021
2022 Senatore, A., Davolio, S., Furnari, L. and Mendicino, G.: Reconstructing Flood Events in
2023 Mediterranean Coastal Areas Using Different Reanalyses and High-Resolution
2024 Meteorological Models, *Journal of Hydrometeorology*, 21(8), 1865–1887,
2025 doi:10.1175/jhm-d-19-0270.1, 2020a.
2026
2027 Senatore, A., Furnari, L. and Mendicino, G.: Impact of high-resolution sea surface
2028 temperature representation on the forecast of small Mediterranean catchments
2029 hydrological responses to heavy precipitation, *Hydrology and Earth System Sciences*,
2030 24(1), 269–291, doi:10.5194/hess-24-269-2020, 2020b.
2031
2032 Seyfried, L., Estournel, C., Marsaleix, P. and Richard, E.: Dynamics of North Balearic
2033 Front during an autumn Tramontane and Mistral storm: air–sea coupling processes and
2034 stratification budget diagnostic, doi:10.5194/os-2018-14, 2018.

2035

2036 Sodemann, H., Aemisegger, F., Pfahl, S., Bitter, M., Corsmeier, U., Feuerle, T., Graf, P.,
2037 Hankers, R., Hsiao, G., Schulz, H., Wieser, A. and Wernli, H.: The stable isotopic
2038 composition of water vapour above Corsica during the HyMeX SOP1 campaign: insight
2039 into vertical mixing processes from lower-tropospheric survey flights, *Atmospheric
2040 Chemistry and Physics*, 17(9), 6125–6151, doi:10.5194/acp-17-6125-2017, 2017.

2041

2042 Stein, A. F., Draxler, R. R., Rolph, G. D., Stunder, B. J. B., Cohen, M. D. and Ngan, F.:
2043 NOAA's HYSPLIT Atmospheric Transport and Dispersion Modeling System, *Bulletin of
2044 the American Meteorological Society*, 96(12), 2059–2077, doi:10.1175/bams-d-14-
2045 00110.1, 2015.

2046

2047 Stocchi, P. and Davolio, S.: Intense air-sea exchanges and heavy orographic
2048 precipitation over Italy: The role of Adriatic sea surface temperature uncertainty,
2049 *Atmospheric Research*, 196, 62–82, doi:10.1016/j.atmosres.2017.06.004, 2017.

2050

2051 Strajnar, B., Cedilnik, J., Fettich, A., Ličer, M., Pristov, N., Smerkol, P. and Jerman, J.:
2052 Impact of two-way coupling and sea-surface temperature on precipitation forecasts in
2053 regional atmosphere and ocean models, *Quarterly Journal of the Royal Meteorological
2054 Society*, 145(718), 228–242, doi:10.1002/qj.3425, 2019.

2055

2056 Strauss, C., Ricard, D., Lac, C. and Verrelle, A.: Evaluation of turbulence
2057 parametrizations in convective clouds and their environment based on a large-eddy
2058 simulation, *Quarterly Journal of the Royal Meteorological Society*, 145(724), 3195–3217,
2059 doi:10.1002/qj.3614, 2019.

2060

2061 Taufour, M., Vié, B., Augros, C., Boudevillain, B., Delanoë, J., Delautier, G., Ducrocq,
2062 V., Lac, C., Pinty, J.-P. and Schwarzenböck, A.: Evaluation of the two-moment scheme
2063 LIMA based on microphysical observations from the HyMeX campaign, *Quarterly
2064 Journal of the Royal Meteorological Society*, 144(714), 1398–1414, doi:10.1002/qj.3283,
2065 2018.

2066

2067 Thévenot, O., Bouin, M.-N., Ducrocq, V., Brossier, C. L., Nuissier, O., Pianezze, J. and
2068 Duffourg, F.: Influence of the sea state on Mediterranean heavy precipitation: a case-
2069 study from HyMeX SOP1, *Quarterly Journal of the Royal Meteorological Society*, 142,
2070 377–389, doi:10.1002/qj.2660, 2015.

2071

2072 Tramblay, Y. and Somot, S.: Future evolution of extreme precipitation in the
2073 Mediterranean, *Climatic Change*, 151(2), 289–302, doi:10.1007/s10584-018-2300-5,
2074 2018.

2075

2076 Turato, B., Reale, O. and Siccardi, F.: Water Vapor Sources of the October 2000
2077 Piedmont Flood, *Journal of Hydrometeorology*, 5(4), 693–712, doi:10.1175/1525-
2078 7541(2004)005<0693:wvsoto>2.0.co;2, 2004.

2079

2080 Uber, M., Vandervaere, J.-P., Zin, I., Braud, I., Heistermann, M., Legoût, C., Molinié, G.
2081 and Nord, G.: How does initial soil moisture influence the hydrological response? A case
2082 study from southern France, *Hydrology and Earth System Sciences*, 22(12), 6127–6146,
2083 doi:10.5194/hess-22-6127-2018, 2018.

2084

2085 Varble, A., Fridlind, A. M., Zipser, E. J., Ackerman, A. S., Chaboureau, J.-P., Fan, J., Hill,
2086 A., McFarlane, S. A., Pinty, J.-P. and Shipway, B.: Evaluation of cloud-resolving model
2087 intercomparison simulations using TWP-ICE observations: Precipitation and cloud
2088 structure, *Journal of Geophysical Research*, 116(D12), doi:10.1029/2010jd015180,
2089 2011.

2090

2091 Verrelle, A., Ricard, D. and Lac, C.: Sensitivity of high-resolution idealized simulations of
2092 thunderstorms to horizontal resolution and turbulence parametrization, *Quarterly Journal*
2093 *of the Royal Meteorological Society*, 141(687), 433–448, doi:10.1002/qj.2363, 2014.

2094

2095

2096 Verrelle, A., Ricard, D. and Lac, C.: Evaluation and Improvement of Turbulence
2097 Parameterization inside Deep Convective Clouds at Kilometer-Scale Resolution,
2098 *Monthly Weather Review*, 145(10), 3947–3967, doi:10.1175/mwr-d-16-0404.1, 2017.

2099

2100 Vié, B., Molinié, G., Nuissier, O., Vincendon, B., Ducrocq, V., Bouttier, F. and Richard,
2101 E.: Hydro-meteorological evaluation of a convection-permitting ensemble prediction
2102 system for Mediterranean heavy precipitating events, *Natural Hazards and Earth System*
2103 *Sciences*, 12(8), 2631–2645, doi:10.5194/nhess-12-2631-2012, 2012.

2104

2105 Vié, B., Pinty, J.-P., Berthet, S. and Leriche, M.: LIMA (v1.0): A quasi two-moment
2106 microphysical scheme driven by a multimodal population of cloud condensation and ice
2107 freezing nuclei, *Geoscientific Model Development*, 9(2), 567–586, doi:10.5194/gmd-9-
2108 567-2016, 2016.

2109

2110 Vincendon, B., Ducrocq, V., Nuissier, O. and Vié, B.: Perturbation of convection-

2111 permitting NWP forecasts for flash-flood ensemble forecasting, *Natural Hazards and*

2112 *Earth System Sciences*, 11(5), 1529–1544, doi:10.5194/nhess-11-1529-2011, 2011.

2113

2114 Winschall, A., Pfahl, S., Sodemann, H. and Wernli, H.: Impact of North Atlantic

2115 evaporation hot spots on southern Alpine heavy precipitation events, *Quarterly Journal*

2116 *of the Royal Meteorological Society*, 138(666), 1245–1258, doi:10.1002/qj.987, 2011.

2117 Wu, F., Cui, X. and Zhang, D.-L.: A lightning-based nowcast-warning approach for short-

2118 duration rainfall events: Development and testing over Beijing during the warm seasons

2119 of 2006–2007, *Atmospheric Research*, 205, 2–17, doi:10.1016/j.atmosres.2018.02.003,

2120 2018.

2121

2122 Vries, A. J. D., 2020: A global climatological perspective on the importance of Rossby

2123 wave breaking and intense moisture transport for extreme precipitation events. *Weather*

2124 *and Climate Dynamics*.

2125

2126 Wyngaard, J. C. and Coté, O. R.: The Budgets of Turbulent Kinetic Energy and

2127 Temperature Variance in the Atmospheric Surface Layer, *Journal of the Atmospheric*

2128 *Sciences*, 28(2), 190–201, doi:10.1175/1520-0469(1971)028<0190:tbotke>2.0.co;2,

2129 1971.

2130

2131 Xie, S.-P., Xu, H., Kessler, W. S. and Nonaka, M.: Air–Sea Interaction over the Eastern

2132 Pacific Warm Pool: Gap Winds, Thermocline Dome, and Atmospheric Convection*,

2133 *Journal of Climate*, 18(1), 5–20, doi:10.1175/jcli-3249.1, 2005.

2134

2135 Ziv, B., Saaroni, H., Romem, M., Heifetz, E., Harnik, N. and Baharad, A.: Analysis of

2136 conveyor belts in winter Mediterranean cyclones, *Theoretical and Applied Climatology*,

2137 99(3-4), 441–455, doi:10.1007/s00704-009-0150-9, 2009.

2138

2139 Zwiebel, J., Baelen, J. V., Anquetin, S., Pointin, Y. and Boudevillain, B.: Impacts of

2140 orography and rain intensity on rainfall structure. The case of the HyMeX IOP7a event,

2141 *Quarterly Journal of the Royal Meteorological Society*, 142, 310–319,

2142 doi:10.1002/qj.2679, 2015.

2143